



The ESA Hera Mission: Detailed Characterization of the DART Impact Outcome and of the Binary Asteroid (65803) Didymos

Patrick Michel¹ , Michael Küppers² , Adriano Campo Bagatin³, Benoit Carry¹ , Sébastien Charnoz⁴ , Julia de Leon⁵, Alan Fitzsimmons⁶ , Paulo Gordo⁷, Simon F. Green⁸, Alain Hérique⁹ , Martin Juci¹⁰, Özgür Karatekin¹¹, Tomas Kohout¹² , Monica Lazzarin¹³, Naomi Murdoch¹⁴, Tatsuaki Okada¹⁵, Ernesto Palomba¹⁶ , Petr Pravec¹⁷ , Colin Snodgrass¹⁸ , Paolo Tortora¹⁹, Kleomenis Tsiganis²⁰ , Stephan Ulamec²¹, Jean-Baptiste Vincent²², Kai Wünnemann²³, Yun Zhang^{1,24} , Sabina D. Raducan¹⁰ , Elisabetta Dotto²⁵, Nancy Chabot²⁶, Andy F. Cheng²⁶ , Andy Rivkin²⁶ , Olivier Barnouin²⁶ , Carolyn Ernst²⁶ , Angela Stickle²⁶ , Derek C. Richardson²⁴ , Cristina Thomas²⁷ , Masahiko Arakawa²⁸, Hirdy Miyamoto²⁹, Akiko Nakamura²⁸ , Seiji Sugita²⁹, Makoto Yoshikawa¹⁵ , Paul Abell³⁰, Erik Asphaug³¹ , Ronald-Louis Ballouz²⁶, William F. Bottke, Jr.³², Dante S. Lauretta³¹ , Kevin J. Walsh³² , Paolo Martino³³, and Ian Carnelli³³

¹ Université Côte d'Azur, Observatoire de la Côte d'Azur, CNRS, Laboratoire Lagrange, CS 34229, F-06304, Nice Cedex 4, France; michelp@oca.eu

² European Space Agency, European Space Astronomy Centre, Camino bajo del Castillo S/N Urbanización Villafraña del Castillo, 28692 Villanueva de la Cañada, Madrid, Spain

³ Universidad de Alicante, P.O. Box 99, 03080 Alicante, Spain

⁴ Université de Paris, Institut de Physique du Globe de Paris, CNRS, F-75005 Paris, France

⁵ Instituto de Astrofísica de Canarias (IAC), University of La Laguna, La Laguna, Tenerife, Spain

⁶ Astrophysics Research Centre, Queen's University Belfast, Belfast BT7 1NN, UK

⁷ Faculdade de Ciências da Universidade de Lisboa, Lisbon, Portugal

⁸ School of Physical Sciences, The Open University, Robert Hooke Building, Walton Hall, Milton Keynes MK7 6AA, UK

⁹ Univ. Grenoble Alpes, CNRS, CNES, IPAG, F-38000 Grenoble, France

¹⁰ Space Research and Planetary Sciences, Physikalisches Institut, University of Bern, Switzerland

¹¹ Royal Observatory of Belgium, Brussels, Belgium

¹² Department of Geosciences and Geography, University of Helsinki, Finland Institute of Geology of the Czech Academy of Sciences, Prague, Czech Republic

¹³ Padova University, Department of Physics and Astronomy, Vicolo dell'Osservatorio 3, I-35122 Padova, Italy

¹⁴ ISAE-SUPAERO, Université de Toulouse, DEOS/Space Systems for Planetary Applications, 10 avenue Edouard Belin, BP 54032, F-31055 Toulouse Cedex 4, France

¹⁵ Japan Aerospace Exploration Agency (JAXA), Institute of Space and Astronautical Science, 3-1-1 Yoshinodai, Chuo-ku, Sagami-hara-shi, Kanagawa 252-5210, Japan

¹⁶ Istituto di Astrofisica e Planetologia Spaziali-INAF, Via del Fosso del Cavaliere 100, I-00133, Rome, Italy

¹⁷ Astronomical Institute of the Czech Academy of Sciences, Fričova 298, CZ-25165 Ondřejov, Czech Republic

¹⁸ Institute for Astronomy, University of Edinburgh, Royal Observatory, Edinburgh EH9 3HJ, UK

¹⁹ University of Bologna, Department of Industrial Engineering, Via Fontanelle 40, I-47121, Forlì (FC), Italy

²⁰ Aristotle University of Thessaloniki, 54124, Greece

²¹ German Aerospace Center (DLR), RB-MUSC, Linder Höhe 1, 51147 Cologne, Germany

²² DLR Institute of Planetary Research, Berlin, Germany

²³ Museum für Naturkunde Berlin, Leibniz-Institute for Evolution and Biodiversity Science, Invalidenstrasse 43, 10115 Berlin, Germany

²⁴ University of Maryland, 4296 Stadium Drive, College Park, MD 20742, USA

²⁵ INAF-Osservatorio Astronomico di Roma, Via Frascati 33, I-00078 Monte Porzio Catone (Roma), Italy

²⁶ JHU/APL, 11100 Johns Hopkins Road, Laurel, MD 20723, USA

²⁷ Northern Arizona University, Department of Astronomy and Planetary Science, PO Box 6010, Flagstaff, AZ 86011, USA

²⁸ Kobe University, Department of Planetology, 1-1 Rokkodai-cho, Nada-ku, Kobe, 657-8501, Japan

²⁹ University of Tokyo, 7-3-1 Hongo, Bunkyo-ku, Tokyo 113-0033, Japan

³⁰ NASA Johnson Space Center, 2101 NASA Parkway, Mail Code XI, Houston, TX 77058-3696, USA

³¹ University of Arizona, 1629 E. University Boulevard, Tucson, AZ 85721, USA

³² Southwest Research Institute, 1050 Walnut Street, Boulder, CO 80302, USA

³³ ESA/ESTEC, Keplerlaan 1, PO Box 299, NL-2200 AG Noordwijk, The Netherlands

Received 2022 January 26; revised 2022 April 25; accepted 2022 April 26; published 2022 July 15

Abstract

Hera is a planetary defense mission under development in the Space Safety and Security Program of the European Space Agency for launch in 2024 October. It will rendezvous in late 2026 December with the binary asteroid (65803) Didymos and in particular its moon, Dimorphos, which will be impacted by NASA's DART spacecraft on 2022 September 26 as the first asteroid deflection test. The main goals of Hera are the detailed characterization of the physical properties of Didymos and Dimorphos and of the crater made by the DART mission, as well as measurement of the momentum transfer efficiency resulting from DART's impact. The data from the Hera spacecraft and its two CubeSats will also provide significant insights into asteroid science and the evolutionary history of our solar system. Hera will perform the first rendezvous with a binary asteroid and provide new measurements, such as radar sounding of an asteroid interior, which will allow models in planetary science to be tested. Hera will thus provide a crucial element in the global effort to avert future asteroid impacts at the same time as providing world-leading science.



Original content from this work may be used under the terms of the [Creative Commons Attribution 4.0 licence](https://creativecommons.org/licenses/by/4.0/). Any further distribution of this work must maintain attribution to the author(s) and the title of the work, journal citation and DOI.

Unified Astronomy Thesaurus concepts: [Near-Earth objects \(1092\)](#); [Asteroid satellites \(2207\)](#); [Impact phenomena \(779\)](#); [Asteroid dynamics \(2210\)](#); [Asteroid surfaces \(2209\)](#)

1. Introduction

The Hera mission is under development in the Space Safety Program of the European Space Agency (ESA) for launch in 2024 October and is based on the previous Asteroid Impact Mission (AIM) concept (Michel et al. 2016). The Hera mission objectives are to investigate from late 2026 December a binary asteroid, including its subsurface and interior properties, and to measure in great detail the outcome of a kinetic impactor test, thus providing extremely valuable information for asteroid impact threat mitigation, mining, and science purposes (Michel et al. 2018).

ESA has been a pioneer in the study of space missions devoted to testing an asteroid deflection technique, starting with the study of the Don Quijote concept in the early 2000s (e.g., Harris et al. 2006), which was originally conceived by Prof. Andrea Milani from the University of Pisa in Italy. This concept involves two spacecraft, one serving as a projectile to impact a small asteroid, the other serving as an orbiter of the asteroid to measure the impact outcome and momentum transfer efficiency of the impact of the first spacecraft. Phase A studies for the Don Quijote mission concept were completed in early 2007, but because no budget or program was associated with this project at ESA, it was then abandoned, until discussions took place about this topic between US and European scientists and agencies in the early 2010s. As a result, NASA and ESA agreed on the study of two independent but related missions, to perform a deflection test using the kinetic impactor technique, along the lines of the Don Quijote concept. These discussions gave birth to the NASA- and ESA-supported Asteroid Impact and Deflection Assessment (AIDA) international collaboration (Cheng et al. 2015; Michel et al. 2016).

The main purpose of AIDA is to support the demonstration and validation of the technology needed to deflect a hazardous asteroid by means of a kinetic impactor, as well as to improve our understanding of the impact process and the momentum transfer to the target asteroid. AIDA will combine the data obtained by two missions. First, the NASA Double Asteroid Redirection Test (DART) will impact the secondary, named Dimorphos, of the binary asteroid (65803) Didymos, and the outcome will be determined with observations by ground-based telescopes (Cheng et al. 2018). In addition, the Light Italian Cubesat for Imaging of Asteroids (LICIACube; Dotto et al. 2021) will be deployed by DART before the impact and will observe the collision and the first few minutes of its aftermath. Second, the ESA Hera mission will rendezvous with the DART mission target and characterize it in great detail, including the crater made by the impactor and the momentum transfer efficiency.

The launch of DART took place successfully on 2021 November 24, 06:21:02 UTC. The impact of the spacecraft on 2022 September 26, 23:14 UTC, will change the orbital period of Dimorphos around Didymos by a minimum of 73 s. As the Didymos–Dimorphos system is a compact system with its binary orbit plane close to the ecliptic, its components mutually eclipse and occult each other twice in every 12 hr orbit. The close proximity to the Earth at the time of impact means that this change of orbital period will be detectable by Earth-bound observers with moderate-size telescopes. The currently known properties of the binary asteroid based on ground-based

observations can be found in Naidu et al. (2020) and in the further update by Scheirich & Pravec (2022).

The original AIM mission studied at ESA until 2016 was supposed to reach Didymos before DART’s impact but did not receive enough funding at ESA’s Council at the Ministerial level in 2016 for its development. On the other hand, the Hera mission, which is an optimized version of AIM, was approved by this Council in 2019 November, but the time for its development and launch in 2024 will lead to its arrival at Didymos 4 yr after the impact. Fortunately, the outcome of the impact is not expected to change in such a short period of time and the main objectives of the mission can be achieved, noting also that LICIACube offers the possibility to observe the impact itself. Hera will perform the first rendezvous with a binary system and its full characterization, while another mission in the NASA SIMPLEX program called Janus was expected to perform a flyby of two asteroid binaries in 2026 (Scheeres et al. 2021), but its launch with the NASA Psyche mission that has been delayed to 2023 may compromise the original plan.

The objectives of Hera related to the deflection demonstration are the following:

1. Measure the mass of Dimorphos to fully determine the momentum transfer efficiency from DART impact.
2. Investigate in detail the crater produced by DART to improve our understanding of the cratering process and the mechanisms by which the crater formation drives the momentum transfer efficiency.
3. Observe subtle dynamical effects (e.g., libration imparted by the impact, orbital and spin excitation of Dimorphos) that are difficult to detect for remote observers.
4. Characterize the surface and interior of Dimorphos, which have great influence on the impact response, to allow scaling of the momentum transfer efficiency to different asteroids.

While Hera is designed as a planetary defense mission, it will also contribute substantially to asteroid science. Beyond the headline results of measuring the effectiveness of the kinetic impactor deflection technology, Hera will also achieve the following:

- (i) Perform the first comprehensive characterization of a binary near-Earth asteroid (NEA), including for the first time its internal properties, allowing a precise comparison with theoretical models and assessment of the binary NEA production mechanism.
- (ii) Constrain the surface structure and regolith mobility on both Didymos and Dimorphos, thereby allowing a first insight into how material properties may affect asteroid satellite formation.
- (iii) Allow, for the first time, the measurement of the detailed surface and subsurface properties of an asteroid crater formed in an impact experiment at an impact speed ($\approx 6 \text{ km s}^{-1}$) that is close to the average speed of interasteroid collisions (Bottke et al. 1994).
- (iv) Provide a remarkable opportunity to study the surface geophysics of two objects of different size and surface gravity, which probably formed from the same material.

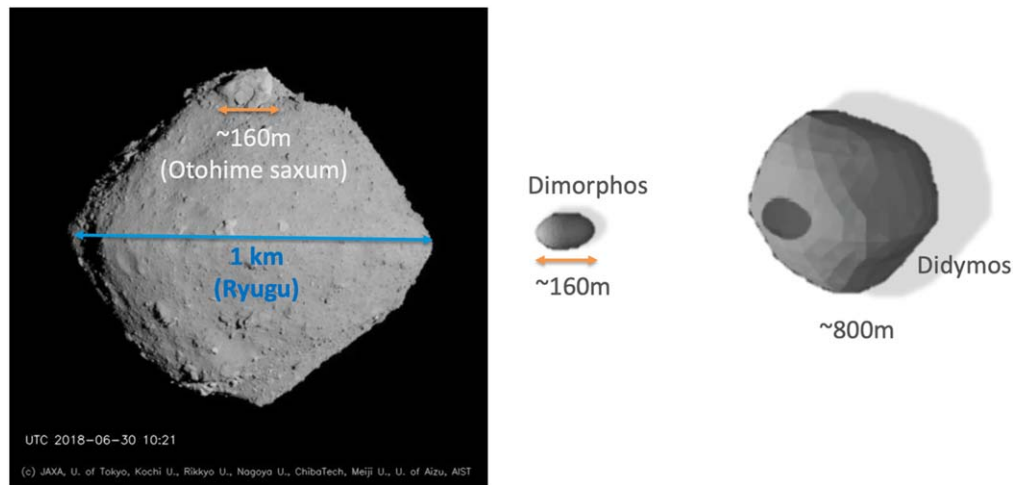


Figure 1. Left: image of the asteroid Ryugu by Hayabusa2's Optical Navigation Camera (ONC) and its biggest boulder, Otohime Saxum. Right: model of the Didymos system. The size of Dimorphos is about the size of the biggest boulder on Ryugu.

- (v) Obtain the first in situ measurements of the properties of an asteroid, Dimorphos, whose size (≈ 160 m diameter) is at the frontier between gravity- and strength-dominated structures.
- (vi) Characterize a crater formed with known energy on a body 160 m in diameter for the first time, allowing us to verify whether strength or gravity is the most influential parameter in crater production on such a small asteroid.
- (vii) Observe for native and post-DART surface activity and particle ejection events.
- (viii) Investigate the crater formed by the DART impact for the potential identification of fresh unweathered material on a silicate asteroid to understand possible space-weathering processes.
- (ix) Test the conclusion that the crater produced by the Small Carry-on Impactor of the Japanese space mission Hayabusa2 on the top-shaped asteroid (162173) Ryugu formed in the gravity regime (Arakawa et al. 2020), by comparing to results of the DART impact onto Dimorphos.
- (x) Investigate an asteroid, Didymos, whose spin period of 2.26 hr may place it at the limit of structural stability (Zhang et al. 2021).

Hera is the first mission designed to rendezvous and characterize a binary asteroid, compare the physical properties of the surface, and determine especially the subsurface and interior structures of the two objects. Past missions to asteroids have revealed their extraordinary diversity in terms of geophysical and compositional properties, but also the extreme geological complexity of each asteroid taken separately. We are still at the stage where we are trying to understand what this complexity tells us about their history and how they respond to the various processes they undergo during their history. Hera will greatly contribute to our understanding of small-body and binary-system geophysics. The possibility of a flyby of another small asteroid, which may also be a binary system, during Hera's cruise to Didymos is still under study and a flyby of Mars, including of one of its small moons, Deimos, is planned. Dimorphos will be one of the smallest (if not the smallest) asteroids visited by a spacecraft (Figure 1) at the time, providing data on geophysics under extremely low gravity

conditions. Furthermore, the DART impact crater provides us with the rare opportunity to study the impact process at solar system scale where both the impact conditions and the crater are accurately known. Finally, the fresh DART impact crater will provide direct access to a subsurface, potentially revealing important new information about the asteroid–meteorite connection and space-weathering effects in the inner solar system.

In the following, we first describe the science addressed by Hera (Section 2), then the instruments that will perform the associated measurements (Section 3), the mission organization (Section 4), and the related Project NEO-MAPP, funded by the European Commission (Section 5), finishing with conclusions and perspectives (Section 6).

2. Science Return

2.1. Impact Physics

Our understanding of impact physics related to asteroids relies on impact and explosion experiments performed on Earth on centimeter-scale targets and on experiments on the real 900 m diameter asteroid Ryugu provided by the Small Carry-on Impactor (SCI; Arakawa et al. 2020) on the Japanese mission Hayabusa2 (Japan Aerospace Exploration Agency (JAXA)); see Section 2.5.

Laboratory experiments are used to validate numerical models at laboratory scale by comparison, generally in terms of the crater's size and depth (or degree of target disruption), as well as ejecta velocity, particle size, and morphology. It is then hoped that, once validated at laboratory scale, these models can be naturally applied to asteroids at geological scales. But this comes with no guarantee, unless a validation at appropriate scale is also performed, hence the significance of the SCI experiment and the DART experiment.

Due to the very low gravity of asteroids such as Ryugu and Dimorphos, numerical impact models have great difficulty in computing the end-to-end cratering process. This is fundamentally because these models are based on shock physics codes, which are appropriate for the more energetic regimes (projectile coupling and shock acceleration of material) but not, without extensive modifications, for the slow granular motion that leads to displacement of asteroid regolith in these low-gravity conditions and the opening of the crater.

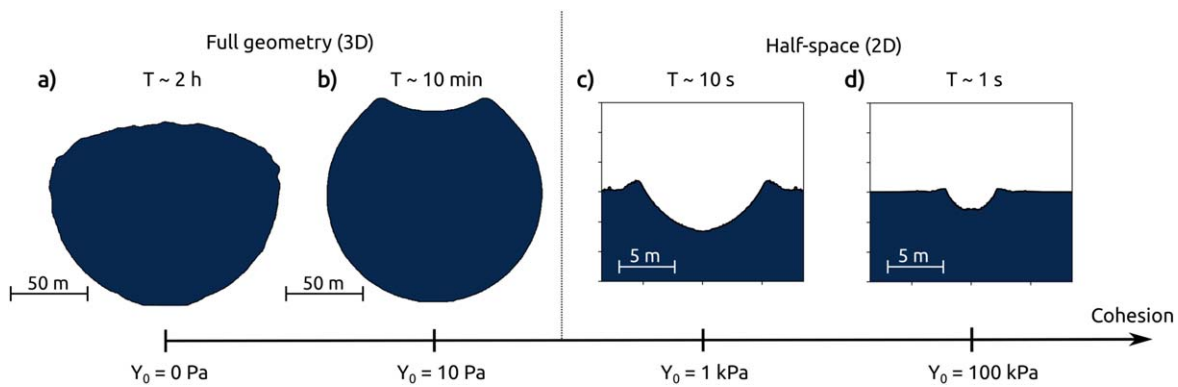


Figure 2. Numerical simulation results: (a, b) Bern’s smoothed particle hydrodynamics or SPH code (adapted from Raducan & Jutzi 2022); (c, d) iSALE-2D (adapted from Raducan et al. 2019) showing the target profile after DART-like impacts into porous Dimorphos-like targets, with varying cohesion (Y_0). DART-like impacts into strong targets ($Y_0 > 1$ kPa) can be modeled using simplified target geometry (half-space). On the other hand, impacts into weak targets ($Y_0 < 1$ kPa), which have a larger cratering efficiency and larger crater formation times (up to 2 hr), require that the entire geometry of the target is numerically resolved. In these impact scenarios, the curvature of the target is important. Moreover, impacts into targets of cohesion less than about 10 Pa create structures dissimilar to cratering, producing global deformation of the target at the same time (Raducan & Jutzi 2022).

The formation of a crater of a given depth takes orders of magnitude longer on a small asteroid than on a terrestrial body, scaling inversely with the square root of the gravity (which scales with radius) in the gravity-controlled regime. If the crater is formed in the strength-controlled regime, the cratering timescale would also be long if the strength is low. So the physics at asteroid scales is complicated and must be computed with sufficient accuracy for much longer timescales.

On asteroids, the final crater properties therefore depend not only on shock, inertia and gravity but also on subtler and more dynamical effects like friction and granular cohesion (Figure 2) and compaction of microporosity. Analytical scaling rules, calibrated with explosive and impact experiments, can be constructed to relate the size of a crater to the size of the impactor, but these assume uniformity of the process and need also to be validated.

Solving for the entire cratering process on small asteroids thus requires an entirely new approach whose validity can only be confirmed with test cases at the relevant scale. The SCI impact offers a first test case, forming a geologically significant crater on asteroid Ryugu at an impact energy corresponding to that of a 2 kg projectile impacting at 2 km s^{-1} . The DART impact will offer a test case in a higher-impact-energy regime involving a 560 kg projectile impacting at 6 km s^{-1} , allowing us also to check the validity of numerical codes at these larger scales and to predict the momentum transfer efficiency.

An asteroid will respond very differently to impacts depending on whether the target is controlled by material strength or gravity, or a combination. Specifically, in the strength-dominated regime, the impact must first disaggregate the rock and overcome shear strength and friction before forming the crater (Holsapple 1993). In the gravity-dominated regime, the target material behaves as a cohesionless medium. As rocks tend to be weaker with increasing size, it is possible that asteroids in the 1 km diameter range are already in the gravity-dominated regime (Asphaug et al. 2002), as found with the SCI impact on Ryugu (Arakawa et al. 2020). The DART impact on a cohesionless Dimorphos would be likely to produce morphologies that are dissimilar to simple cratering events and would change the global morphology of the asteroid (Raducan & Jutzi 2022).

Since numerical simulations are computationally very expensive, we often need to derive from laboratory experiments

empirical scaling rules that relate observable parameters to material properties and impact conditions. There is even a debate about whether cratering experienced on the smallest asteroids (≈ 100 m in diameter) may be in a fundamentally different mechanical environment and thus not adequately explained by even the strength-regime scaling (e.g., Jutzi 2015; Raducan et al. 2019).

The morphological analysis of DART’s impact location is fundamental for calibrating our models of impact physics. Hera will give us the first measurements for an impact speed of 6 km s^{-1} on a small asteroid’s surface of all the following morphological parameters: crater depth, crater diameter, presence of a raised crater rim and its height, and area of any ejecta blanket. From measurements of these features, theoretical models can then be validated or revised. DART itself will not observe the crater, and its companion, the Italian LICIACube, is also unlikely to determine the final dimensions of the crater owing to the very high speed of its flyby and the expected presence of a large ejecta plume shortly after impact. However, LICIACube will give us precious information on the early ejecta produced by the impact, which are also a test for numerical models (Dotto et al. 2021).

Hera will thus allow for the first time the measurement of the detailed properties of the target of an impact, including its surface and subsurface properties that have a great influence on the impact response, and the detailed morphology and size of a large crater performed at the actual scale of an interasteroid collision with the same speed (DART impact speed of 6 km s^{-1}) as those between asteroids (about 5 km s^{-1} on average). The impact conditions will be known (DART impact), the early outcome of the impact will also be observed by LICIACube, and the post-impact outcome will be precisely measured by Hera.

As an example of application of impact-modeling validation, the age of a planetary surface is estimated from the counting and size distribution of impact craters, and then from the time needed to produce such a distribution on the considered surface, given a known impactor size distribution and impact frequency. A crucial parameter is thus the relation between the crater’s size and the projectile’s size (for a given impact speed). If this relation is flawed, then the age estimate will be flawed too. This exercise done on Ryugu and Bennu from Hayabusa2 and OSIRIS-REx images, respectively, showed that the age can

differ by orders of magnitude depending on the relation used to derive it (Sugita et al. 2019; Walsh et al. 2019; Arakawa et al. 2020; Ballouz et al. 2020).

Another example is the question of how much impact energy leads to a given degree of disruption. Typically, in collisional-evolution or planet-formation models, criteria relying on ad hoc or numerical modeling parameters are used to define how much damage is produced when two bodies collide and whether cratering or disruption occurs. Hera will tell us whether the assumed parameters are consistent with the new knowledge acquired thanks to the new measurements at the impact energy of DART, with possible profound implications for our understanding of the collisional evolution in different eras of solar system history.

Along the same lines, the influence of impacts on asteroid dynamics is not well understood (e.g., how much of the energy may be transferred into the rotational energy of the target?). The measurement of the DART impact outcome in terms of the dynamical properties of the target, in particular its rotation state (noting that it should be well characterized from the ground before the DART impact), will provide crucial information on the contribution of impacts to the dynamics of a small asteroid.

Hera and DART/LICIACube will thus provide a fully documented impact outcome at the scale of an asteroid under low-gravity conditions and will allow numerical models and scaling rules to be validated or revised so that they can be applied with higher reliability to other cases and crucial problems in planetary science.

2.2. Geophysics at Very Low Gravity

When Hera reaches Dimorphos, it will investigate one of the smallest asteroids (if not the smallest) ever observed by spacecraft. So far, three asteroids less than 1 km in diameter have been explored by space missions: Itokawa (535 m \times 294 m \times 209 m) by Hayabusa (JAXA), Bennu (505 m \times 492 m \times 457 m) by OSIRIS-REx (NASA), and Ryugu (1023 m \times 986 m \times 438 m) by Hayabusa2 (JAXA). Each observation revealed very different geophysical characteristics. Itokawa displays a large variety of terrains, from smooth areas to regions covered with pebbles and boulders. Bennu and Ryugu share a similar spinning top shape but differ significantly in local morphology (local slopes, number and shape of craters, presence of smooth deposits, ridges), as well as in composition (Ryugu appears to hold far less water than Bennu, and the relation between spectral colors and space weathering seems to work in an opposite way: DellaGiustina et al. 2020; Tatsumi et al. 2021). These different morphologies and properties highlight the range of complex formation mechanisms and evolutionary processes affecting asteroids.

The small lander MASCOT aboard the Hayabusa2 mission provided in situ data from the surface of Ryugu (Ho et al. 2021) showing different kinds of surface textures in high-resolution images (Jaumann et al. 2019), as well as rocks with very high porosity and a low tensile strength in the few hundred kPa range (Grott et al. 2019). Furthermore, the sampling of Bennu by the Touch And Go SAMpling Mechanism (TAGSAM) of OSIRIS-REx revealed that the surface of the asteroid, as a result of its low gravity, behaves like a granular bed with near-zero cohesion that is half as dense as the bulk asteroid (Laretta et al. 2022; Walsh et al. 2022). An internal cohesive strength of only a few tens of Pa was found to be required to prevent the disruption of the fast-spinning kilometer-diameter NEA

(29075) 1950 DA (Rozitis et al. 2014). Clearly, the behavior of small asteroids in their low-gravity environment challenges our intuition and requires direct interactions to be captured.

By performing a rendezvous with the Didymos system, Hera will characterize a new class of objects (binaries) and provide us with the opportunity to directly test both binary formation and asteroid evolution scenarios (see Section 2.3).

Despite the fact that Ryugu and Bennu belong to spectral classes different from Didymos, they all have in common their top shape, according to radar observations of the latter. The former are classified into the wide C class, whose analog meteorites are carbonaceous chondrites. Didymos, instead, belongs to the S class, which includes asteroids whose analog meteorites are the ordinary chondrites. Such shape analogy had been already noticed in other C- and S-class top-shape NEAs, such as (175706) 1996 FG3 and (66391) Moshup, which are both binary NEAs belonging to different spectral classes, with primary top shapes revealed by radar observations. A common mechanism is apparently shaping NEAs into top-shape bodies with or without satellites, irrespective of their composition. The Hera mission will largely contribute to the understanding of such a process.

Direct observation of a binary system will also improve our assessment of where asteroids such as Bennu and Ryugu fit in relation to binary asteroids (Figure 1). For example, are some asteroids in the process of becoming binaries? Or have some asteroids been binaries previously and lost their companion?

Images of Didymos will show us the fastest-spinning object ever visited, with a spin period of only 2.26 hr. Depending on its level of surface cohesion, Didymos may actually be on the margin of structural stability (Figure 3; Zhang et al. 2017, 2021) and may still lose particles from its surface. Hera offers the possibility to observe for the first time an object that is possibly still reshaping, losing mass, and not yet in its final configuration.

Hera will determine precisely the shape and mass (and its distribution) of the DART impact target, from which we will derive a detailed slope map of the surface. As the topography is controlled by a competition between strength and gravity, we will thus obtain a measure of the internal strength of Dimorphos, which is related to the inner structure. Hera will also be capable of determining the shape of Didymos. Destabilization of slopes and regolith migration is evident on all asteroids visited so far (Murdoch et al. 2015; Jawin et al. 2020). From Hera's observations of regolith mobilization and ponding associated (or not) with local slopes, we can identify gravitational anomalies or discrepancies in the distribution of density. The analysis of gravity anomalies and regolith size distribution can provide key insights into the internal structure of the body and the binary formation process. In particular, regolith size distribution on the surface of the primary body may provide indications about the formation process and internal structure of Didymos and thus constrain the binary formation mechanism.

The precise shape, mass, and interior measurements of Dimorphos made by Hera will provide density constraints that are crucial for estimating the asteroid's porosity. These measurements can point to the presence of high-density materials in the interior or the presence of large voids. Hera's porosity measurements are also relevant for understanding the cratering process on asteroids: porous materials exhibit less

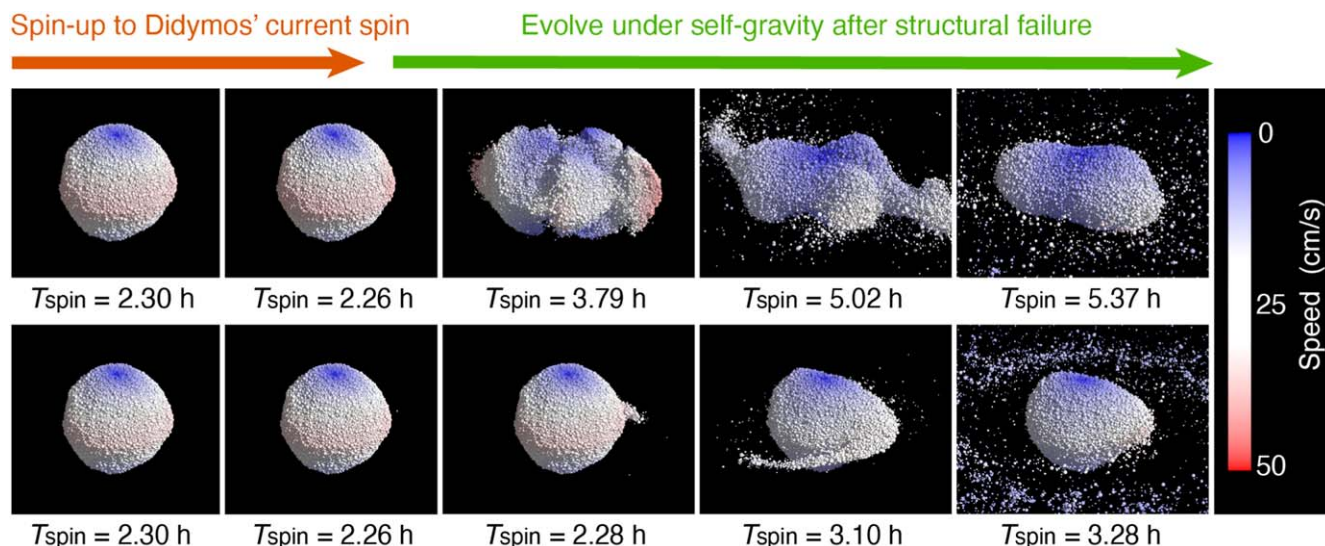


Figure 3. Numerical modeling of Didymos-shaped rubble piles' evolution under spin-up by the YORP effect, a torque caused by the scattering of sunlight and reemission of thermal radiation from an irregularly shaped body (Rubincam 2000), showing the sensitivity of the structural stability to the spin state and the different possible evolutionary pathways (adapted from Zhang et al. 2021). Top: a strength-dominated case with a bulk density of 1820 kg m^{-3} and bulk cohesion of $\sim 39.0 \text{ Pa}$; bottom: a gravity-dominated case with a bulk density of 2170 kg m^{-3} and bulk cohesion of $\sim 15.0 \text{ Pa}$. Particles are color-coded by their translational speeds. The spin period T_{spin} of the body is given below each frame. The body was subject to spin acceleration in the beginning and then evolved without external influence after its structure failed (as indicated by the two long arrows; the spin rate decreases in the reconfiguration process owing to angular momentum conservation). In both cases, the rubble-pile structures can be stable at Didymos's current spin with a small increment of $\sim 0.5 \text{ Pa}$ in the bulk cohesion. The results were obtained by soft-sphere discrete-element modeling using the numerical code `pkdgrav` (Schwartz et al. 2012).

relaxation after impact, resulting in larger depth-to-diameter ratios with respect to solid rocks (Housen & Holsapple 2003).

Although natural craters are less obvious on rubble piles than on other rocky surfaces, they can be found and have been counted on Itokawa, Ryugu, and Bennu (Hirata et al. 2009; Daly et al. 2020; Cho et al. 2021). Hera will measure the size–frequency distribution of impact features on Dimorphos. This will allow estimates to be made of the age of the surface of Didymos and Dimorphos thanks to cratering scaling rules adapted from the DART impact outcome. Such estimates will also indicate whether craters are being eroded by, e.g., seismic activity (Marchi et al. 2015; Murdoch et al. 2015).

Crater morphology—their degradation state and ejecta—gives information on the mechanical properties of the body (Housen & Holsapple 2003; Asphaug 2008). By comparing a fresh crater (due to the DART impact) with older features, we will be able to characterize the speed of erosion and crater erasure for the first time, setting a very strong constraint on how asteroid surfaces evolve. Combined with spectral measurements, we can relate this morphological evolution to the general effects of space weathering.

The extremely low gravity on the surface of Dimorphos implies that cohesion, electrostatics, or other forces may dominate regolith dynamics (Scheeres et al. 2010). However, Bennu and Ryugu were found to be very different from the expectations based on those same arguments. The relative importance of these forces with respect to surface gravity depends on various parameters, such as the regolith particle sizes, which makes it extremely difficult to estimate a priori. Studying those regions where avalanches occur and where particles accumulate can provide indications about the frictional properties of the grains and on their cohesive and electrostatic properties.

Additionally, asteroids are subject to geomorphic alteration by seismic energy (e.g., Richardson et al. 2005; Murdoch et al. 2015) in response to collisions. When a smaller asteroid strikes

another, it produces a crater, but it also generates a complex seismic source whose energy is confined to the relatively small volume of the target. Depending on attenuation, the seismic energy can have global effects on crater degradation (e.g., Thomas & Robinson 2005; Asphaug 2008). Seismic disturbance by the SCI experimental impact (a 2 km s^{-1} , 2 kg impactor) on asteroid Ryugu was not immediately noticeable (Arakawa et al. 2020), but subsequent analysis showed that most of the boulders within 15 m of the impact were slightly displaced by seismic shaking, with surface disturbances evident up to 40 m (Honda et al. 2021). The DART impact is thus expected to have strong global seismic signatures on Dimorphos, whose proper interpretation can provide information about the asteroid's structural interior and behavior.

In summary, Hera will provide not only a detailed characterization of a fast-spinning top shape and one of the smallest solar system bodies ever visited but also a remarkable opportunity to study two objects of different size formed, very likely, by the same material. This knowledge is fundamental not just for understanding the response of a body to a deflection attempt but also for understanding the geophysical evolution of asteroids in general and constraining surface ages. Additionally, in characterizing the surface geology of both Didymos and Dimorphos, Hera offers a fantastic opportunity to understand the influence of the surface gravity on asteroid regolith behavior and surface evolution.

2.3. Binary Formation

Although currently less than 350 of the more than a million known small bodies have been identified as binary or multiple systems, around $15\% \pm 4\%$ of NEAs are estimated to be binaries (e.g., Pravec & Harris 2007; Margot et al. 2015). Not only does this mean that Earth gets a double impact every so often (the 36 and 26 km diameter Clearwater Lakes craters in Canada, for example; see also Oberbeck 1973; Melosh et al.

1996; Cook et al. 2003; Miljković et al. 2013; Lagain et al. 2020; Wren & Fevig 2020), but also their properties provide important clues to solar system evolutionary and dynamical processes (e.g., Walsh & Jacobson 2015). For example, once a binary system is identified and the separation distance and orbital period are measured, the mass of the system can be estimated, in the manner that Newton famously estimated the masses (and thereby densities) of Earth, Jupiter, Saturn, and the Sun in *Principia*.

Although there were already multiple indications for asteroids being binary, the first proof of a satellite in orbit around an asteroid was the discovery of Dactyl orbiting the large main-belt asteroid (MBA) (243) Ida after the flyby of the Galileo mission en route to Jupiter in 1993 (Belton et al. 1996).

The range of properties of NEA binaries is less broad than found for MBAs, but this is probably a result of the restricted size of NEAs rather than their different dynamical histories. Four main classes of binary asteroids have been defined (Pravec & Harris 2007) and updated (Walsh & Jacobson 2015). Among NEAs, the most common binaries are so-called Group A, consisting of small (diameter $D < 20$ km) asteroids with a secondary-to-primary-diameter ratio (D_s/D_p) ranging from 0.1 to 0.6 (with typical mass ratios of a few percent), in close orbits (semimajor axis $a < 9D_p$). Group B has similar properties but larger satellites ($D_s/D_p > 0.7$), whereas Group W has wider separations ($a > 9D_p$). The fourth group, L, consists of larger asteroids ($D_p > 20$ km) like (243) Ida, and therefore they are only found in the MBA population, with relatively small satellites ($0.2 < D_s/D_p < 0.7$).

The evolution of MBAs is dominated by collisions, with only the largest bodies (diameters larger than several tens of kilometers) remaining undisrupted since their formation, as evidenced by dynamical and collisional models, the asteroid size distribution, cratering rates, and the presence of asteroid families (groups of asteroids with clustered orbital parameters); see Holsapple (2022) for a review. The distribution of spin rates, with absence of objects of kilometer and larger diameter rotating faster than the limit for strengthless bodies, coupled with low density/high porosity, implies that the majority of asteroids less than 100 km across are highly fractured or rubble piles (gravity-dominated aggregates of collisional fragments; Campo Bagatin et al. 2001).

Asteroid families provide the strongest evidence for catastrophic collisions (Farinella et al. 1982; Michel et al. 2001). Collisional models reveal that reaggregation following collisional disruption (e.g., Michel et al. 2001) is a more common formation mechanism than bound ejecta from subcritical impacts, for the L-group MBA binaries (see Bottke et al. 2015, for a review). The smallest monolithic fragments and aggregates (below a few tens of kilometers in diameter) are dispersed through the Yarkovsky effect (asymmetrical scattering/reemission of sunlight), causing changes in their orbital semimajor axes, putting them in unstable zones such as the 3/1 mean-motion resonance with Jupiter or the ν_6 secular resonance, which convey them to the near-Earth region on a million-year timescale by increasing their orbital eccentricity (e.g., Gladman et al. 1997; Bottke et al. 2002; Granvik et al. 2018). This provides a mechanism for the continual replenishment of the NEA population, which is considered to be in a steady state, based on the analysis of craters and related impact flux on the Moon, despite the 10 Myr median lifetime of its members (Gladman et al. 2000).

Tidal forces have been seen to disrupt small bodies (as in the case of Comet Shoemaker–Levy 9 after a close encounter with Jupiter in 1992; Asphaug & Benz 1996). However, although the orbits of NEAs allow close encounters with the terrestrial planets, the distance at which tidal effects become important is very small (Zhang & Michel 2020), and the properties of most binary NEAs are not consistent with formation by tidal disruption. Elongated primaries with moderate spin periods and secondaries with eccentric orbits expected from tidal disruption do not match the observed properties of typical binary NEAs, in particular the oblate spheroidal shape with an equatorial bulge (spinning top shape) of their primaries, and their lifetimes before separation are very short (Walsh & Richardson 2006; Walsh et al. 2008). In addition, small MBAs, which do not have close planetary encounters, also show binarity. Spin rates near the fission limit are also not consistent with binary formation following an asteroid disruption, capture through a three-body interaction, or capture after a catastrophic impact. Instead, they are indicative of formation from a rotational fission event (e.g., Margot et al. 2002; Pravec & Harris 2007).

Binary formation among the NEA population, as well as for small MBAs, appears to be driven by disruption from spin-up due to the YORP effect. This effect, which has decreasing efficiency with increasing heliocentric distance and which is also extremely sensitive to surface features (Statler 2009), can cause small asteroids to spin up to their fission limit, where the small amount of self-gravity and cohesive forces holding the asteroid together are overcome by rotational acceleration. At this point, depending on the failure mode of the progenitor (Figure 3; Zhang et al. 2021), loose material at the equator can no longer be retained by the asteroid, which starts losing mass. The YORP effect spinning up asteroids has now been observed acting on several NEAs (e.g., Lowry et al. 2007; Hergenrother et al. 2019). A variety of mechanisms proposed for YORP-induced binary formation, from fission (Scheeres 2007) to shedding of material that then reaggregates in orbit (Walsh et al. 2008), are consistent with the observed properties of binary NEAs, with primaries spinning close to the fission limit, and secondaries in close, near-circular equatorial orbits. The spinning top shape can then be the result of spin-induced mass shedding, reshaping, and either remnants of material resulting from slow mass loss or deposition of debris from breakup of fission components in orbit. However, such shapes may not always be linked to binary formation but can also result from parent body disruption and reaccumulation (Campo Bagatin et al. 2020; Michel et al. 2020).

Another side effect of YORP is the reorientation of spin axes to obliquities of either 0° or 180° . Not only is this observed for many single NEAs, but it also is apparent in the spin and orbit axes of NEA binaries (La Spina et al. 2004). Earth-based optical and radar observations have shown that the Didymos–Dimorphos system shares this orientation. Therefore, Hera will provide our first laboratory to test model predictions of this important and ubiquitous evolution pathway for NEAs.

After binary formation, the evolution of the system can result in a range of outcomes, depending in part on the initial mass ratio q of the secondary to primary (Jacobson & Scheeres 2011). The result can be stable binary or multiple systems, recombination, or separation to form unbound asteroid pairs. The latter are observed as pairs of asteroids with similar orbits and properties consistent with a common formation (e.g.,

Pravec et al. 2010). The threshold between bound and unbound systems is at $q \approx 0.2$. For $q < 0.2$ (which is the case for Didymos) the system is unbound, and the dynamical evolution following rotational fission of the parent body leads to a chaotic binary that may disrupt or may undergo rotational fission of the secondary, followed by re-impact of one component onto the primary, forming a top-shaped primary with an equatorial bulge. The binary YORP (BYORP) effect, in which the orbital properties of a binary asteroid evolve under radiation torques mostly acting on a tidally locked secondary (i.e., with spin period synchronous with its orbital period), causes an increase or decrease in the semimajor axis of the binary orbit, eventually resulting in merger or separation. However, tidal forces and libration of the secondary add complications to the process and can change or suppress the effects of BYORP. Wide (W-type) binary systems can be explained in terms of this effect.

The Hera mission will provide the first close-up observation of an NEA binary asteroid that is predicted to have formed by YORP. It will provide detailed measurement of the post-impact orbit of Dimorphos, as well as unique global observations of properties of both components not possible during the short DART encounter. Measurement of the mass of Dimorphos is key not only to interpreting the changes in orbit for planetary defense purposes but also in testing dynamical models to understand the evolution of binary systems in general. The detailed shapes of the primary and secondary, as well as their thermophysical properties, determine the strength of the YORP and BYORP torques. The observed mass and volume derived from shape models allow the density/porosity of the secondary to be compared with that of the primary. Such estimations, together with inferred internal structure, confirmation of synchronous rotation, degree of libration if not too largely altered by DART impact, precise orbital eccentricity, and morphological properties from imaging, will help constrain the binary formation mechanism and test evolutionary models by providing a well-constrained example.

Imaging of the top-shape primary can provide evidence for surface material mobility (e.g., boulder tracks, freshly exposed unweathered material, size sorting) or reshaping (e.g., local slope variation, crater distortion) that also yield clues to the physical evolution of small fast-spinning asteroids, as already demonstrated by the OSIRIS-REx and Hayabusa2 space missions to top-shape asteroids (Lauretta et al. 2019; Watanabe et al. 2019). The detailed morphology of the equatorial ridge, together with detection or constraints on orbital particles (distinguished dynamically from any remaining DART impact ejecta), will constrain any current level of activity or cohesive forces that prevent it and may reveal its formation as a source or sink of orbital material.

While Hera plays a vital role in the determination of the post-impact dynamics and material properties required for verification of the kinetic impactor technique, its measurements thanks to a rendezvous will provide the first ground truth to constrain formation and evolutionary processes of binaries, many of which also drive the dynamical and physical evolution of all small asteroids.

2.4. Relevance for Overall Properties of Asteroids

As indicated above, Hera will provide new and important science applicable to general studies of asteroids in the solar system. Previous missions have characterized silicate asteroids over a range of sizes: NASA Near-Shoemaker to Eros (34×11

km), Galileo at Gaspra (18×9 km), NASA Stardust at Annefrank (7×3 km), and JAXA Hayabusa at Itokawa (0.5×0.2 km). Hera will allow in-depth characterization of a 160 m diameter body (Dimorphos), as well as the primary Didymos (800 m in diameter). Comparing the regolith of both binary components with the surfaces of the near-Earth carbonaceous asteroids Ryugu (as seen by Hayabusa2) and Bennu (as seen by OSIRIS-REx) will be especially important. Once new data were obtained from these two missions, the estimates of surface ages of these two bodies changed by at least an order of magnitude from the initial estimate based on the first pictures (Sugita et al. 2019; Walsh et al. 2019; Arakawa et al. 2020; Ballouz et al. 2020), showing that we do not yet have a coherent understanding of the surfaces of small asteroids; the in-depth studies by Hera of Didymos and Dimorphos will provide critical data to untangle the various physical processes that operate in these environments.

A current understanding, supported by the analyses of Itokawa's samples returned by the Japanese mission Hayabusa (Nakamura et al. 2011), is that the surfaces of silicate asteroids (S-type taxonomy) become chemically altered over time owing to high-energy particles and micrometeoroid bombardment. Such space weathering changes spectral properties, making surfaces optically darker and redder and reducing the contrast of silicate absorption bands. Fresh asteroid surfaces (Q-type taxonomy) share the same spectral characteristics as ordinary chondrites recovered on Earth's surface. Within the near-Earth population, a range of surfaces exist, from old weathered S-type surfaces to relatively fresh Q-type asteroids. But it is difficult to disentangle the fast particle weathering over timescales up to 1 million yr (Brunetto et al. 2015), the slower micrometeoroid impact timescale of 100 million yr, and the various resurfacing processes such as YORP spin-up, gardening of the regolith by larger impacts, thermal degradation of rocks (Delbo et al. 2014), and tidal encounters.

The only previous flyby of a fresh Q-type asteroid, when NASA Deep Space 1 encountered asteroid Braille, was unfortunately hampered by instrumental problems (Buratti et al. 2004). As Didymos is an S-type asteroid, it is assumed that Dimorphos will also be of a similar surface composition, but unweathered material probably exists right below the surface. The depth at which such material may lie is dependent on the history of the binary system. The DART impact may uncover this subsurface of unweathered silicate material on Dimorphos, as seen in the interiors of ordinary chondrites recovered on Earth's surface. Hence, Hera could be the first spacecraft to characterize unaltered Q-type silicate material in its original environment. At the same time, the dynamical and geological studies will provide important information for constraining the timescale of space weathering.

The in-depth study by Hera of the DART crater will have an additional benefit. The cratering event by NASA Deep Impact on comet 9P/Tempel 1, and its subsequent imaging by the follow-up NASA Stardust-NExT mission, allowed impact models on low-density icy surfaces to be calibrated for the first time (Schultz et al. 2013), although the identification of the crater was done after the comet passed perihelion, which may have modified its surface morphology. As a natural consequence of the planetary defense studies of the DART crater, Hera will provide a cornerstone linking impact energy to crater measurement on rocky asteroids, as described above (see Section 2.1). This, in turn, will allow refined exploration of

impact history on asteroid surfaces visited by spacecraft, both past and future.

The correlation between asteroid size and spin state was one of the most important discoveries in asteroid science. It is observational evidence that over 99.9% of asteroids with diameter between 300 m and 10 km have spin periods greater than 2.2 hr (Pravec & Harris 2000). This shows that asteroids in this size range are only weakly bound owing to self-gravity and cohesive forces, being heavily fractured or rubble piles (see also Section 2.1). Below 100 m in diameter, asteroids show a broad range of spin periods ranging from minutes to days. Originally it was believed that this indicated that smaller asteroids are coherent (solid) objects, in agreement with catastrophic disruption scaling (e.g., Melosh & Ryan 1997; Benz & Asphaug 1999). Indeed, the boulder at the south pole of Ryugu, Otohime Saxum (Figure 1), is near this size (Watanabe et al. 2019), and the largest boulder on Bennu (Roc Saxum) is also 100 m in longest apparent dimension. Nonetheless, recent theoretical considerations of intergrain molecular (van der Waals) forces, together with measurements of lunar regolith, suggest that part of the asteroid population at the small size end may be rubble piles (Sánchez & Scheeres 2014). Dimorphos will be the first asteroid visited by a spacecraft that lies at the size threshold between the two spin populations, so there is no way to argue what is the most likely internal structure of Dimorphos and whether it is dominated by strength or gravity. Hera will give insight into the true general nature of small asteroid interiors.

Finally, there are over 1.1 million asteroids now cataloged by astronomers. The majority of known MBAs have diameters >1 km owing to sensitivity limits of current survey telescopes. The future Vera Rubin Telescope, scheduled to begin operations in 2023, will perform the first complete survey below 1 km diameter throughout the main asteroid belt and will reach 100 m diameter objects in the inner belt within 2.5 au of the Sun. Hence, for the first time, comparison will be possible between NEAs the size of Didymos and Dimorphos and the large population of similarly sized objects in the main belt. The understanding Hera gives us of asteroids in this size range will become directly applicable to similar asteroids in the main belt, either in their own stable orbits or near resonances and on their own path to becoming NEAs.

2.5. Relation to Hayabusa2 and OSIRIS-REx Sample-return Missions

One of the striking findings of the two sample-return missions (Hayabusa2, JAXA, and OSIRIS-REx, NASA) that simultaneously visited their asteroid targets (Ryugu and Bennu, respectively) is the similarity of the shape of these targets. Both are top-shape asteroids with similar bulk density. Both also have an apparent concentration of craters at the equator. The top shape is common, according to radar observations, for primaries of binary systems, including Didymos (Figure 1). Several studies show that such a shape is intimately linked to the formation of a natural satellite via YORP spin-up (see Section 2.3). However, it was recently found that this can also be the natural outcome of the formation of small asteroids by catastrophic disruption and reaccumulation (Michel et al. 2020). Now, the big question is, did Ryugu and Bennu have a natural satellite in the past? Answering this question will have big implications for the history of these bodies and therefore for the interpretation of the samples that were and will be returned

to Earth in 2020 and 2023, respectively. By comparing the surface and internal properties of Didymos measured by Hera with those of Bennu and Ryugu (e.g., the ridge structure, the regolith/boulder distribution, the internal density distribution), it will be possible to add new constraints to the evolution of these two asteroids. Furthermore, clues on the formation of such shapes and the potential former presence of a natural satellite may be revealed. Had Ryugu and/or Bennu any such satellite, they were lost at some point, explaining the current lower spin rate of both bodies as compared to the one needed to lose surface material. Hera will thus provide us with information that may open new perspectives regarding the data interpretation from other science missions.

Another important result is also fully relevant to Hera. On 2019 April 5, Hayabusa2 successfully performed an impact experiment on the surface of Ryugu, by launching a 2 kg projectile at 2 km s^{-1} on the asteroid. Measurements of the ejecta production were performed by a small camera called DCAM3, and the crater's dimensions were later measured by Hayabusa2 and its ONC camera. Its diameter is estimated to be about 15 m (Figure 6, Arakawa et al. 2020), while numerical models and scaling laws predicted a diameter of a few meters at most, assuming a strength-dominated surface. The current interpretation is that the crater was produced in the gravity regime and the surface is basically cohesionless despite the presence of apparently solid boulders at the impact site. Extrapolating centimeter-scale laboratory experiments to asteroid scales and the modeling of impact physics in the gravity regime, when gravity is so low, remain a challenge. Furthermore, while the SCI projectile was shot at 2 km s^{-1} , DART will impact at about 6 km s^{-1} . Even if material properties of Ryugu and Dimorphos are not expected to be the same, the possibility to compare two impact experiments at two different impact speeds will feed the important question of how crater parameters scale with impact speed. This, in turn, will provide new and important constraints on some parameters used in cratering scaling laws that rely on this scaling with impact speed. This will have major implications in understanding cratering histories of small bodies, asteroid regolith creation, and gardening.

Finally, the interaction of the OSIRIS-REx sampling tool (TAGSAM), which made a slow impact into the surface of Bennu, also revealed the very low cohesion and density of the surface of the asteroid (Lauretta et al. 2022; Walsh et al. 2022). Furthermore, although there is some indication of subsurface stiffness (Barnouin et al. 2019), impact craters on Bennu may also be controlled by either gravity scaling or strength scaling assuming a very low strength (<100 Pa), except for small craters that are affected by armoring (Bierhaus et al. 2022).

Thus, after careful analysis of the data acquired by Hayabusa2 and OSIRIS-REx and the various interactions on their surface by both missions, it seems that the gravity regime of impact craters dominates both Bennu and Ryugu. This is contrary to the original expectations and explains the revision of surface ages of both bodies from the first published estimates (Sugita et al. 2019; Walsh et al. 2019) to the latest ones (Arakawa et al. 2020; Ballouz et al. 2020; Bierhaus et al. 2022).

In summary, Hayabusa2 and OSIRIS-REx have revealed the geological complexity of their two visited asteroids and their unexpected mechanical behavior, allowing us to make a giant step in our understanding of those bodies. Adding newly obtained knowledge by OSIRIS-REx and Hayabusa2,

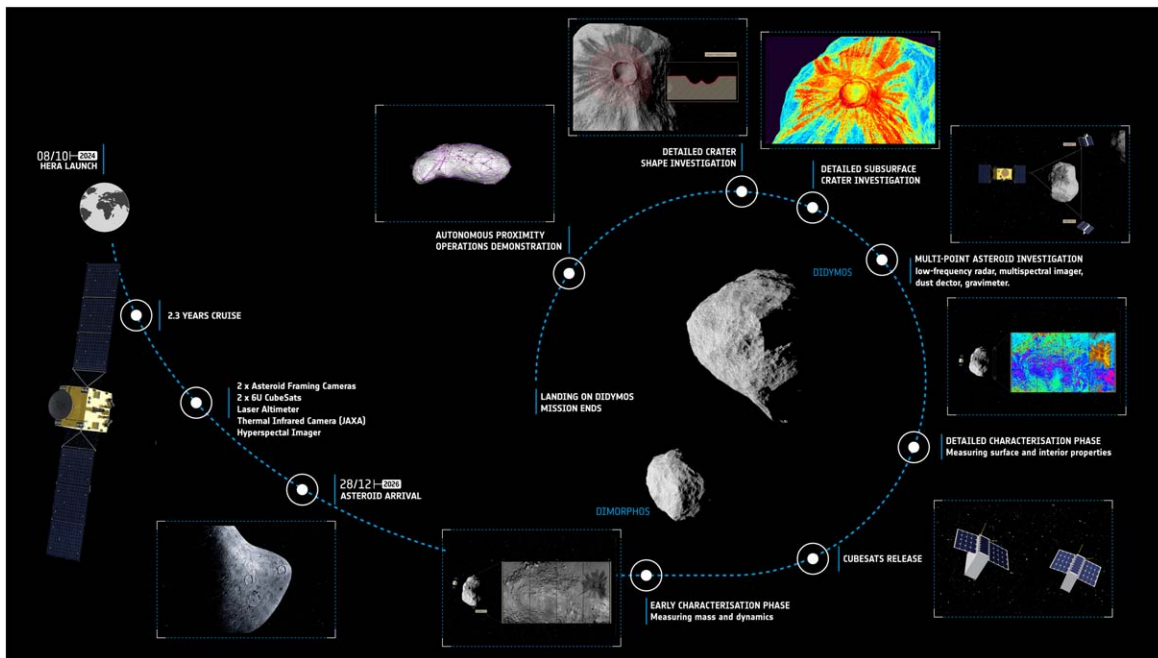


Figure 4. Overview of the Hera mission at the Didymos system.

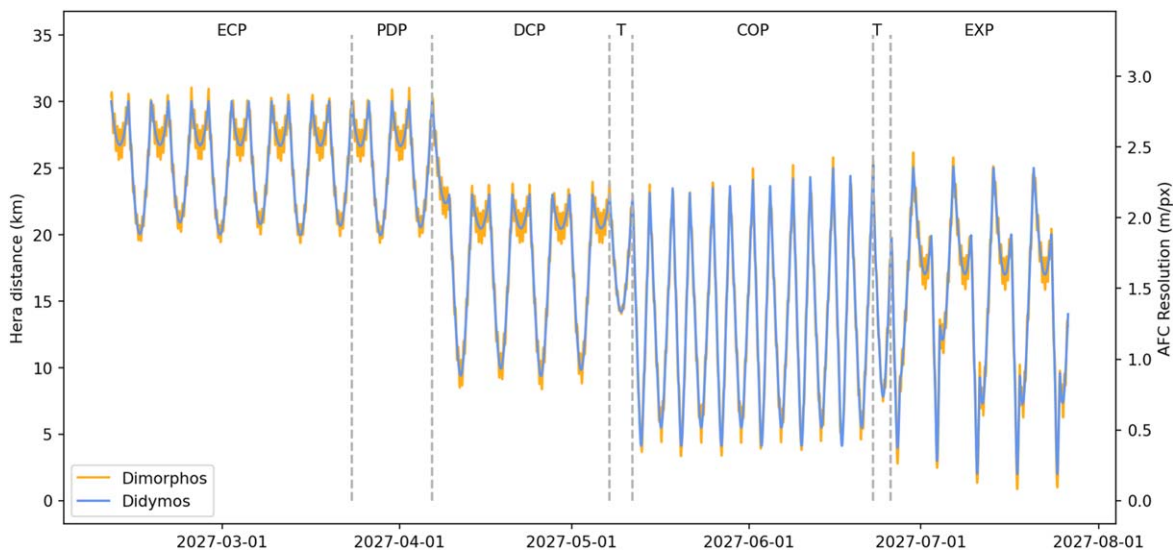


Figure 5. Distance from Hera to Didymos/Dimorphos and AFC image resolution. ECP: Early Characterization Phase; PDP: Payload Deployment Phase; DCP: Detailed Characterization Phase; COP: Close Observation Phase; EXP: Experimental Phase; T: Transitions.

concerning both top-shape single asteroids and impact craters, to that provided by Hera on a binary top shape, concerning outcomes of the DART impact experiment on Dimorphos, a much smaller object than Ryugu or Bennu with measurements of Dimorphos’s physical characteristics, will make the total knowledge gained by these missions much greater than the sum of the parts!

3. Mission Overview

Hera will be launched in 2024 October, with the launch window opening on the 8th of October and closing on the 25th. The baseline launcher is an Ariane 6.4, with a Falcon 9 launcher as backup. After a deep-space maneuver (DSM) 2–3 weeks after launch, Hera will swing by Mars in 2025 March at a minimum altitude of 5000–8000 km. A second DSM in 2026

January brings Hera on course to Didymos. In addition to a flyby of the martian moon Deimos during the flyby of Mars, a possible asteroid flyby during cruise is being investigated. At arrival, the capture sequence consists of five maneuvers, beginning on 2026 December 14 and ending with orbit insertion at the end of January or early February 2027.

Backup launch opportunities exist in 2025 and 2026. In both cases, arrival at Didymos would be late 2030 or early 2031.

An overview of the mission at Didymos is given in Figure 4. The distance between Hera and Didymos during the proximity operations is shown in Figure 5. After orbit insertion, the following mission phases are defined:

1. *Early Characterization Phase* (6 weeks). The Early Characterization Phase starts at orbit insertion and consists of hyperbolic arcs at distances of typically 20–30 km from

the asteroids. Short arcs of 3 days' duration are interleaved with long arcs taking 4 days, creating a weekly cycle. During this phase, the global shape and mass/gravity, as well as thermal and dynamical properties, of both asteroids will be determined, in preparation for the next phases. The Early Characterization Phase will also be used to define target regions for close flybys during the Close Observation and Experimental phases. The design of this phase is similar to Rosetta operations after orbit insertion around comet 67P/Churyumov–Gerasimenko (Taylor et al. 2017).

2. *Payload Deployment Phase* (2 weeks). The focus of the Payload Deployment Phase is the release of the two CubeSats and the support of their early operations. The trajectory type followed by Hera is the same as during the Early Characterization Phase.
3. *Detailed Characterization Phase* (4 weeks). During the Detailed Characterization Phase, Hera continues to move on hyperbolic arcs, utilizing the same repeatable weekly scheme as during the Early Characterization Phase. The distance to the asteroids is reduced to 8–20 km. While the previous phases were flown with ground navigation, the closer distances of the Detailed Characterization Phase require at least partly autonomous attitude guidance, utilizing the position of Didymos for navigation. The Detailed Characterization Phase is used for meter-scale mapping of the asteroids and determination of thermal, spectral, and interior properties. It will also be used for multipoint measurements with Hera and its two CubeSats.
4. *Close Observation Phase* (6 weeks). The Close Observation Phase continues with the operations scheme of the previous phases, but reducing the pericenter distance to 4 km. This requires full autonomous attitude guidance and, below a distance of 8 km, when Didymos starts overfilling the field of view of the camera, feature tracking needs to be enabled for navigation and/or the cameras need to switch to Dimorphos. The Planetary ALTimeter (PALT) laser will start to be used for navigation. This phase, with a total of 12 close flybys, will be used for high-resolution investigations of a large fraction of the surface area of Dimorphos, including the DART impact crater.
5. *Experimental Phase* (6 weeks). The previous mission phases up to the Close Observation Phase provide opportunities to meet all Hera mission requirements. In the Experimental Phase, innovative navigation techniques are used to get flybys to lower altitudes, down to 1 km or less. In the Experimental Phase, autonomous attitude and trajectory guidance will be demonstrated, requiring a combination of feature tracking and distance measurements with PALT. The Experimental Phase will reach a resolution of decimeters in morphological, spectral, and thermal properties of Dimorphos at selected targets, including the DART impact crater. The Experimental Phase and the Hera mission will end with the Hera spacecraft landing on Didymos, providing high-resolution data on the primary in the process.

4. The Hera Spacecraft

The Hera spacecraft is built by an industrial consortium led by OHB System AG. Its design is shown in Figure 6. With a

total mass of ≈ 1280 kg, it is a small-to-medium-size planetary spacecraft. Its architecture is based on a central tube and adapter cone. It is powered by 13 m^2 of solar panels. It is equipped with a fixed high-gain antenna and two low-gain antennas. Communications with ground stations utilize X band. In addition, an intersatellite link is used for communications between Hera and its CubeSats using S band, with a maximum range of 60 km. Its bi-propellant chemical propulsion will provide a Δv of $\approx 1300\text{ m s}^{-1}$. It contains 16 thrusters for orbit control and 6 more for reaction control.

Hera is three-axis stabilized. Attitude is maintained by four reaction wheels, as well as gyros, star trackers, Sun sensors, and the Asteroid Framing Cameras (AFC). In addition, the Planetary Altimeter (PALT) will be employed for attitude guidance.

5. Payload

To accomplish its goal and produce the expected planetary defense and science knowledge, the Hera spacecraft will carry several instruments whose use is defined in the Science Traceability Matrix (Table 1).

The onboard instruments of the Hera mission are:

1. Two Asteroid Framing Cameras (AFCs)
2. A Spectral Imager (Hyperscout-H)
3. A microLIDAR (PALT)
4. A thermal Infrared Imager (TIRI)
5. An X-band transponder referred to X-DST in Section 5.5 and a Hera-to-CubeSats Intersatellite Link (ISL) transceiver for the radio science experiment (RSE).

In addition, Hera will carry two CubeSats that will be deployed at close proximity to Dimorphos and will communicate with the mother craft through the ISL transceiver mentioned above. The two CubeSats are as follows:

1. Juventas, composed of the low-frequency monostatic radar JuRa, which will perform the first direct measurement of an asteroid interior, as well as the gravimeter for small solar system objects (GRASS), an accelerometer, and the ISL.
2. Milani, composed of the near-infrared imager ASPECT, the VISTA microthermogravimeter, and the ISL.

In the following we describe the main characteristics of each of these instruments.

5.1. Asteroid Framing Cameras

The Asteroid Framing Cameras (AFC) are a set of two identical imaging systems with a two-dimensional detector. Their main purpose is navigation and scientific activities requiring observations of the target asteroid system from multiple positions and from various distances during the course of the mission. Figure 5 shows in more detail how the imaging resolution will change during the mission.

The AFCs are built by JenaOptronik and are based on their Astrohead cameras.³⁴ The cameras are equipped with the FaintStar 1020×1020 pixel CMOS Active Pixel Sensor. The opticals system provides a total field of view of 5.5×5.5 deg. The expected instantaneous field of view (IFOV, i.e., angular resolution per pixel) is $94.1\ \mu\text{rad}$. Those specifications are

³⁴ <https://www.jena-optronik.de/products/star-sensors/astrohead.html>

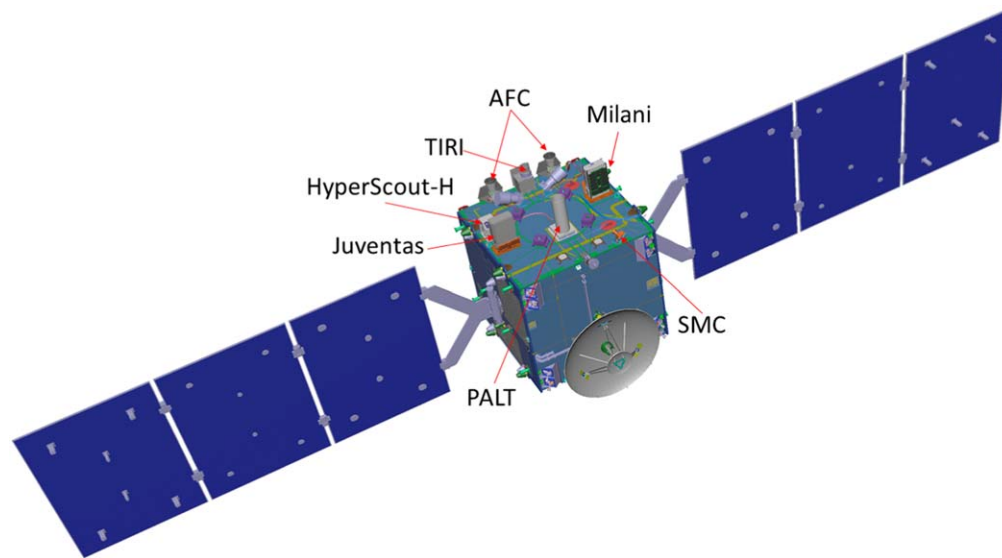


Figure 6. Hera spacecraft design. The locations of the different payload elements are indicated (AFC = Asteroid Framing Cameras; TIRI = Thermal InfraRed Imager; PALT = Planetary ALTimeter; SMC = Small Monitoring Cameras).

Table 1
Science Traceability Matrix for Hera

Mission Requirement	High-level Product	Contributing Payloads
Mass of Dimorphos and dynamical properties of the Didymos system	Dimorphos orbital state	AFC, PALT, TIRI, RSE, GRASS, ISL
	Gravitational acceleration	AFC, PALT, RSE, GRASS, ISL
	Satellites/debris/dust ejection	AFC, TIRI, ISL, VISTA
	Nongravitational acceleration	AFC, TIRI, RSE
Global properties, interior structure	Shape/volume (global, + high-res DART crater)	AFC, PALT
	Internal structure, density and porosity distribution	AFC, RSE, JuRa, ISL
Characterization of the surface properties	Geomorphology (global description of the surface)	AFC, TIRI, JuRa, ASPECT
	Mechanical properties (strength, angle of friction, density, cohesion, etc., derived from local and geomorphological studies)	AFC, PALT, TIRI, JuRa, GRASS, GNC, ASPECT
	Optical and thermal properties	AFC, PALT, TIRI, Hyperscout-H, ASPECT, VISTA
	Composition and space weathering	TIRI, Hyperscout-H, JuRa, ASPECT, VISTA
Additional high-level products	Maps, common references (e.g., names, frames, coordinates)	all

chosen to fulfill all imaging requirements designed for the mission: global mapping of both asteroids at spatial scales of $2\text{--}3\text{ m pixel}^{-1}$ in the Early Characterization Phase, $1\text{--}2\text{ m pixel}^{-1}$ in the Detailed Characterization Phase, and $0.5\text{--}2\text{ m pixel}^{-1}$ in the Close Operation Phase. In addition, dedicated flybys over selected areas of high scientific interest (e.g., the DART crater, the JUVENTAS landing site) will bring the resolution down to 10 cm pixel^{-1} .

The AFC contributes to all science aspects of the mission as listed in Table 1. More specifically:

1. The AFC will contribute to the measurement of Dimorphos's mass by providing the necessary data to evaluate the dynamical properties of both asteroids. The AFC will acquire light curves of the system while in cruise phase, search for debris and small satellites that could be hazardous but also inform us on the gravitational

field around the binary system, and then map both objects and track surface features in order to derive the rotational state of each object.

2. The global maps provided by AFC will be a basis to reconstruct the tri-dimensional shape of Didymos and Dimorphos, down to a spatial scale of 50 cm on the 3D model. The 3D reconstruction of the topography will be calculated with state-of-the art stereophotogrammetry (mostly *shape from motion*, tracking similar features across multiple images with varying viewing geometry) and completed with stereophotoclinometry (*shape from shading* when we have an accurate photometric function to describe the surface regolith). Shape modeling is a necessary step to calculate the volume of each object and, coupled with mass determination from radio science, determine their density and internal structure.

- From images and topography, the AFC contributes to the description of the asteroids' morphology, on global (regions, feature size distributions, slopes, etc.) and local (boulders, craters, regolith movement, etc.) scales. The AFC is a panchromatic camera: it acquires a signal integrated over a spectral range of 370–1100 nm and therefore will not provide detailed spectra. However, careful cross-calibration with Hyperscout should allow the camera to obtain albedo measurements on the surface at high spatial resolution (10 cm pixel⁻¹).

5.2. Hyperscout-H Spectral Imager

The Hyperscout-H spectral imager used on Hera is based on the hyperscout-1 imager performing Earth observations on the GOMX-4B CubeSat. Its large field of view combined with the Linear Variable Filter (LVF), designed for Earth observations, would complicate the operations for an asteroid mission. Therefore, the LVF is being replaced by a mosaic filter.

Hyperscout-H will provide spectral images of Didymos and Dimorphos in the visible–near-IR wavelength range diagnostic for identifying different asteroid spectral classes. It will allow searches for evidence of variation in space-weathering effects (subtle spectral slope and silicate feature strength differences) from the DART impact crater, ejecta deposition, and possible resultant surface movement on Dimorphos, as well as spin-induced resurfacing processes on Didymos.

Hyperscout-H features a 2048 × 1024 pixel CMOS detector with the mosaic filter attached to the detector. The filter contains 25 spectral bands in the wavelength range 665–975 nm (see Figure 7). The field of view is 16° × 8°. The pixel scale is 133 μrad pixel⁻¹; the effective spatial resolution will be between the pixel resolution and the size of the 5 × 5 macropixel representing the 25 spectral bands, depending on the extent to which the original resolution can be restored by demosaicking.

5.3. PALT

The Hera LIDAR, designated PALT (Planetary ALTimeter), performs range measurements that will be used to support asteroid 3D topography, fall velocity, wobble of the asteroid (rotation measurements), and target albedo (the instrument measures the power of the received pulse, making it possible to calculate the target reflectivity). Also, the instrument can be used to support near-asteroid navigation.

PALT is a time-of-flight (TOF) altimeter that provides time-tagged distances and velocity measurements. It is based on a Laser Landing Altimeter Engineering Model and is developed by EFACEC (Portugal and Romania), Synopsis Planet (Portugal), and INOE (Romania). PALT has two modules, the optical box (see Figure 8) assembled on the exterior of the satellite and the electronics box assembled inside the satellite. The optical box comprises a microchip laser and a low-noise sensor. The synergies between these two technologies enable the development of a compact instrument for long-range measurements with a low power consumption. The optical box includes the receiver, emitter, and associated electronics. The receiver has a Cassegrain telescope with a 70 mm diameter primary mirror and a refractive module (positioned below the primary mirror) that includes a sensor. The laser-emitter module includes the beam-expanding optics and the laser. The laser source is a compact low power consumption

microchip laser that emits 2 ns pulses with energies of 100 μJ and wavelength of 1.5 μm. PALT provides time-tagged distance measurements, with a measurement range of 14 km to 500 m, an accuracy of 0.5 m, and a mass below 1.5 kg. The electronics has four main blocks: power supply, processing unit, front-end, and TOF and opto-mechanics interfaces. Power supply is optimized for the altimeter secondary power consumption and output filtering. The processing unit is based on a Field Programmable Gate Array (FPGA) since it simplifies the process of keeping precise timing, required to operate the TOF unit. FPGA is also responsible for performing all the housekeeping acquisitions, to monitor the health of the altimeter, and for the interface with the spacecraft, via serial communication. TOF is the key block of the LIDAR altimeter with respect to its accuracy and precision. This unit is responsible for time-tagging all the laser-emitter pulses, as well as all the avalanche photodiode (APD) receptions, with a precise timed tag that will then be managed by the processing unit FPGA to compute the distance. The front-end electronics is responsible for the laser power supply and triggering and for the laser pulse digitalization (emitted and received). PALT acquisition modes can be made in BURST or SINGLE mode; in BURST mode the instrument will output a measurement at a configurable periodicity (maximum 10 Hz). In both working modes, PALT will also periodically send a housekeeping packet with the equipment health information.

5.4. TIRI

The Thermal Infrared Imager (TIRI) is developed by JAXA, inherited from the thermal imager TIR on Hayabusa2 (Okada et al. 2017), which observed the C-type NEA 162173 Ryugu (Okada et al. 2020). TIRI is based on an uncooled microbolometer array of 1024 × 768 effective pixels and has a field of view of 13.3 × 10.0 deg., covering the whole binary system from 20 km distance. The angular resolution is 0°013 pixel⁻¹, corresponding to 5 m pixel⁻¹ from 20 km altitude, or 0.5 m pixel⁻¹ from 2 km altitude. The observable temperature ranges from 150 to 400 K to simultaneously observe the surfaces on both the dayside and the nightside from large solar phase angles. Thermal imaging (thermography) is the main function of TIRI, but thermal infrared multiband imaging is also its function with an eight-position filter wheel: one position for a wideband filter of 7–14 μm for thermal imaging; six positions for narrowband filters centered at 7.8, 8.6, 9.6, 10.6, 11.65, and 13.1 μm to determine the Christiansen feature and the Reststrahlen feature (Salisbury et al. 1991), which indicate the surface material composition or meteoritic types; and one position used as a shutter and the reference temperature plate.

TIRI is used to investigate thermophysical properties of the surface of an asteroid, especially for the surface particle size distribution and for the surface thermal inertia of boulders, which is related to microporosity. In the Hayabusa2 mission, the highly porous nature of the surface boulders and their surroundings on Ryugu, investigated using the TIR instrument, seem to be a typical characteristic for C-type asteroids (Okada et al. 2020; Shimaki et al. 2020). TIR also discovered some cold boulders with typical thermal inertia of carbonaceous chondrites (Okada et al. 2020) and some hot spots inside craters that seem to be anomalously porous boulders (Sakatani et al. 2021). TIR was also used to track the deployed small impactor and to find the target marker (Okada 2020). In the Hera

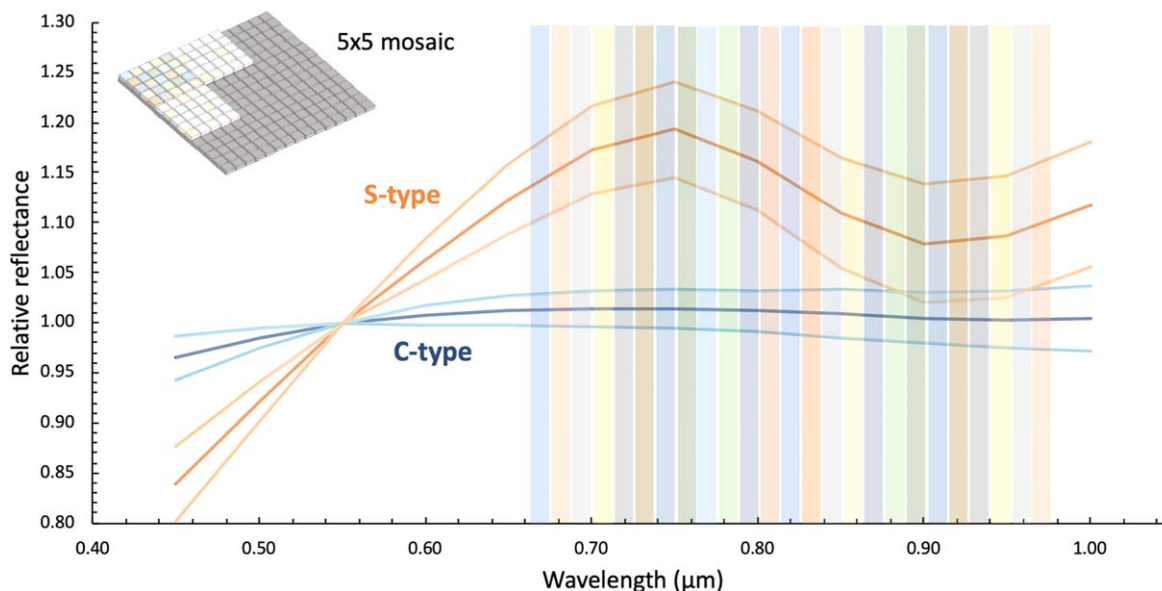


Figure 7. Schematic showing the wavelength coverage by the filters on Hyperscout-H. Also shown are average spectra of S-type and C-type asteroids.

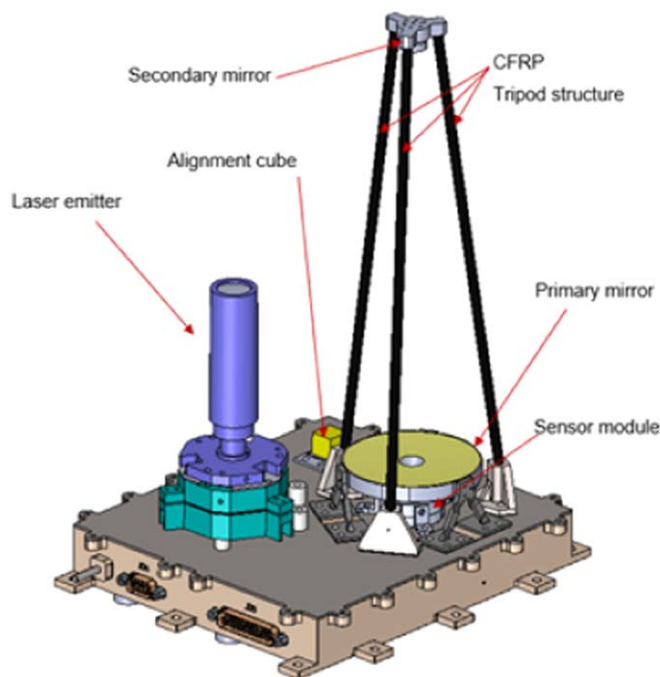


Figure 8. PALT optical box design.

mission, TIRI will investigate the spatially resolved thermo-physical properties of an S-type asteroid for the first time. Such physical properties provide key information on the strength of materials under microgravity conditions (Grott et al. 2019). TIRI will also map the thermal properties of the smallest asteroid ever explored. Using the multiband functions, TIRI will also compare the materials of Didymos and Dimorphos and map the composition difference between the inside and outside of the artificial crater excavated by the DART impact. By constructing the thermal models of Didymos and Dimorphos derived from the thermal images, TIRI will contribute to understanding of the orbital and rotational evolution processes of asteroids by the Yarkovsky and YORP effects and the dynamical evolution of a binary system by the

BYORP effect. Thermal images capture the whole asteroid, including the nightside, which is helpful in constructing a precise shape model and for navigating the spacecraft at large solar phase angles.

5.5. X-DST for Radio Science

The X-DST will provide the standard capability for simultaneous sending of housekeeping telemetry data and receiving telecommands from ground. In addition, it will support two-way range, range-rate, and Delta-Differential One-Way Ranging (Delta-DOR) tracking from Earth ground stations.

The X-DST will give a maximum contribution to the end-to-end Allan standard deviation of 8 for a 60 s integration time (2×10^{-15} at 1000 s integration time), which yields a relative speed error contribution of $2.4 \mu\text{m s}^{-1}$ at 60 s integration time ($0.6 \mu\text{m s}^{-1}$ at 1000 s). Ranging data will be affected by the following maximum ranging error contributions: 3.4 ns (100 cm) for the high-frequency noise, 3 ns (90 cm) for the calibration error, and 3 ns (90 cm) for aging and drift. These specifications are fully in line with the RSE requirements, which were set in the detailed study carried out when the Hera mission was still being studied under the name AIM (Zannoni et al. 2018).

Hera's X-DST includes an additional board inside the Digital Module to support Wide Band Delta Differential One-way Ranging (WBDDOR). With the F1 frequency defined as 9.586 4 MHz (according to communication channel respecting Hera specifications), two Delta-DOR tones at $F1/2$ and $2 \times F1$ are supported by the X-DST as follows: (a) the low-frequency tone at $F1/2$ is synthesized in the DST Application-Specific Integrated Circuit (ASIC) and modulated onto the carrier in the digital domain, and (b) the high-frequency tone at $2 \times F1$ is synthesized in the DST ASIC and modulated onto the carrier directly at X band. WBDDOR analysis, simulations, and breadboarding were carried out in the frame of two ESA studies, with results reported in Cardarilli et al. (2019).

The long-term behavior of the binary system is mainly affected by nongravitational forces like the YORP effect and

the BYORP effect. In order to derive a realistic model of the system's evolution, both of these effects require an excellent knowledge of the masses of the bodies involved. This knowledge will be acquired via the RSE with Hera, involving the main spacecraft and the CubeSats (Tortora et al. 2019, 2020; Zannoni et al. 2020; Tortora et al. 2021). However, to determine the YORP and BYORP effects, a key observable is the one coming from spacecraft angular measurements, where the novel WBDDOR system will be a key enabling technology boosting the determination accuracy. The Hera mission will be the first mission to perform an in-flight demonstration of the WBDDOR capabilities.

5.6. Intersatellite Link for Radio Science

The main goal of the ISL transceiver is to guarantee the correct communication (sending telecommands and receiving telemetry) between the Hera mother craft and the CubeSats Juventas and Milani. However, the direct communication between these three objects offers a unique opportunity to carry out, for the first time, a radio science experiment involving precise range-rate measurements between the CubeSats and the mother craft.

Most of the information about the formation processes of an asteroid lies in its interior structure. The bulk density can be inferred by measuring the mass and volume, both of them accessible with a spacecraft orbiting the asteroid or performing close flybys, equipped with a camera and a radio tracking system. In particular, the determination of masses and gravity fields requires an orbit determination process solving simultaneously for the spacecraft trajectory and the asteroid mass and gravity field. However, while ground-based S/C radio tracking is a well-established technique for relatively large and massive bodies, the use of space-to-space intersatellite links capable of determining the Doppler shift due to the relative line-of-sight velocity between the two bodies would be much more appropriate at small bodies, but this technology has not been explored much. Our previous studies (Tortora et al. 2019, 2020, 2021; Zannoni et al. 2020) have shown that the satellite-to-satellite tracking option would ideally complement ground-based radio tracking, providing the best results for both the mass and gravity field determination and S/C positioning. Hera will, for the first time, use a miniaturized and lightweight ISL system, capable of being integrated on nanosatellites weighing a few kilograms. The specifications of this system include (a) bidirectional data exchange, (b) line-of-sight range measurements (ranging), (c) range-rate, and (d) time correlation. For most of these capabilities, the ISL system seems perfectly in line with the technical requirements imposed by the Hera baseline scenario. However, the range-rate accuracy capability is currently undergoing a significant improvement, in order to contribute substantially to the Hera gravity science experiment. The ISL to be flown on Hera will incorporate a high-precision range-rate mode, capable of an end-to-end accuracy of $50 \mu\text{m s}^{-1}$ at 60 s integration time, and this should allow the estimate of Dimorphos's standard gravitational parameter (GM) and J2 (the gravity coefficient that measures the oblateness) within 0.1% and 10%, respectively, and Didymos's gravity field, up to degree 3.

It is expected that the high-precision range-rate mode of the ILS on the Milani CubeSat (Section 5.8) will not provide a significant contribution to the RSE because of the larger CubeSat distance from Dimorphos, as compared to the

Juventas CubeSat (Section 5.7). However, the standard range-rate, ranging, and Telemetry, Tracking and Control (TT&C) functions will be used to control and navigate the CubeSat during its operational life.

5.7. Juventas

Juventas is a 6U CubeSat developed by a consortium led by GomSpace and devoted to the geophysical characterization of Dimorphos. The main objectives are

1. to determine the gravity field of Dimorphos;
2. to determine the interior structure of Dimorphos;
3. to determine the surface properties of Dimorphos.

To achieve these objectives, the CubeSat is composed of the following payloads.

5.7.1. The Low-frequency Monostatic Radar JuRa

JuRa (for Juventas Radar) will be devoted to the first investigation of a binary asteroid interior. The radar is a monostatic synthetic aperture radar operating at low frequency to sound the asteroid interior, with heritage from the radar developments done in the context of the AIM mission (Herique et al. 2018, 2019). JuRa transmits a Binary Phase Shift Keying (BPSK) coded signal with a 20 MHz bandwidth, a 60 MHz carrier, and 5 W peak power. A fast burst of thousands of transmissions and receptions is performed, and the received signal is accumulated on board to increase the signal-to-noise ratio. For each measurement, a first burst transmits one linear polarization and receives the two linear polarizations on separate channels; then, a second burst transmits the other linear polarization and receives both. With the 60 MHz carrier frequency and the measurement repetition, JuRa should provide global returns from inside the bodies of Didymos and Dimorphos (see Herique et al. 2018 for detailed discussion).

In comparison to space-borne radars designed to sound Mars or the Galilean satellites, this small radar is optimized to operate at low altitude and low relative speed, with an increased versatility. The antennas are two crossed dipoles (Figure 9) formed by 1.5 m long booms. The large antenna aperture allows the instrument to illuminate the whole binary system during operations at 2 km distance without detailed pointing maneuvers. Full-linear polarization capabilities allow JuRa to compensate the variation of the dipole-antenna gain as a function of the direction separately for each linear polarization, to achieve radiometric calibration of the measurements.

From 2027 April, JuRa will provide the first direct measurement of an asteroid's internal structure, covering both Didymos and its moon Dimorphos with a baseline resolution of 15 m or better. JuRa will map the returned power per surface or volume unit, quantified by the backscatter coefficient usually called σ_0 . For any penetrating radar, the texture of the scattering area, the size of the heterogeneities, and the corresponding dielectric contrast drive the propagation regime of the radar waves, their penetration, the statistics of the received signal, and the information it contains. In other words, the properties of the internal structure are the driving quantities for the propagation regime, the properties of the received signal, the inversion approach to be considered, and also the method to simulate the measurement. It is also the main

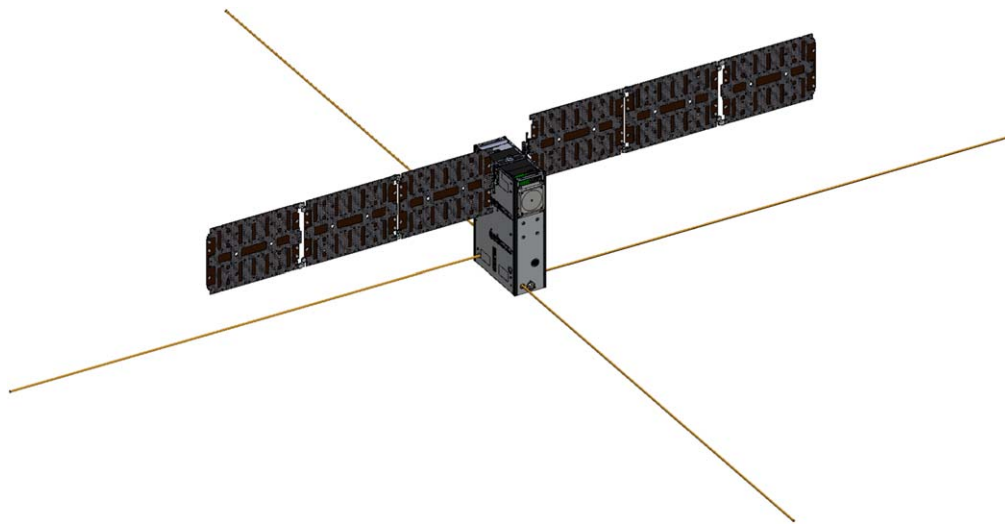


Figure 9. The Juventas small platform with the four JuRa antenna booms as deployed for JuRa operations (courtesy of GomSpace Luxembourg Sarl).

unknown for asteroids and definitely the main question addressed by JuRa.

This first sounding of an asteroid represents the opening of a new field of asteroid investigation. The definition of the processing and products remains notional and requires different scenarios to be considered in parallel, with a different focus depending on what the asteroid has in store for us. For instance, with two sequences of operations of a month each with a mean orbit radius of 3.3 km and then 1.9 km, a revisit of more than 20 passes might allow JuRa to resolve a global 3D image, to identify internal features and spatial heterogeneity of the constitutive materials, if the asteroid is transparent to hundreds of meters at 60 MHz (Gassot et al. 2021).

The first objective of JuRa is to characterize Dimorphos's interior, to bring out the aggregate structure and to characterize its heterogeneity in terms of contrast and size distribution at scales from 20 cm to 20 m. Knowing the size of the constituent blocks and the size of the voids, as well as the presence of fine dust or gravel filling the voids, provides strong constraints on the presence and fraction of macroporosity versus microporosity.

The spatial variation of the received signal allows JuRa to identify internal geological structures such as layers, larger blocks or voids, subaggregates, and significant spatial variation of the density, porosity, or block size. Such information will provide significant constraints on the mechanical model of the DART impact process (Section 2.1). However, it should be noted that a direct detection of the DART-induced mass redistribution in the vicinity of the crater is not expected considering the 10–15 m JuRa resolution.

The second objective is to estimate the average permittivity and to monitor its spatial variation in order to retrieve information on the moonlet composition and porosity (Herique et al. 2016). With a wavelength of ~ 1 m, the JuRa radar largely bypasses the near-surface alteration layering produced by space weathering and thermal cycling that influences optical remote sensing. A partial penetration through the interior, e.g., tens of meters, will provide a measurement of dielectric constants and an indirect estimation of the permittivity contrast. A full penetration of the whole moonlet, e.g., hundreds of meters, will allow a direct measurement of the average permittivity and a 3D tomography of the permittivity (Sava & Asphaug 2018; Kofman et al. 2020),

The same characterization will be applied to the primary (Didymos) of the binary system, as a secondary objective, to detect differences in structure and composition. A comparison of signal statistics received from Didymos and Dimorphos will demonstrate the presence of segregation processes and deformations during moon formation in a binary system, helping to discriminate between progressive and catastrophic processes and to model the stability conditions of the system.

Finally, the radar data processing requires an accurate determination of the geometry of observation of the spacecraft and the observed target (orbits, rotations, libration, mutation) with decametric relative accuracy. Autofocus methods are usually applied to radar data to estimate and correct geometry unknowns. This part of the JuRa processing ground segment will be developed in collaboration with HERA Working Group 4 (see Section 6) to evaluate the possible contribution of JuRa to support the determination of the dynamical properties of the Didymos system.

5.7.2. The Gravimeter GRASS

GRASS is being developed to measure the local acceleration vector on the surface of Dimorphos. Following the soft landing of the Juventas CubeSat on Dimorphos, GRASS will record the temporal variation of the surface gravity vector at the landing location. GRASS will be the first gravimeter ever on an asteroid.

The gravimeter is being developed by the Royal Observatory of Belgium, together with EMXYS and GomSpace. The heritage is from the Asteroid Geophysical Explorer (AGEX) study as part of the ESA CubeSat Opportunity Payload Intersatellite Network Sensors (COPINS) of the ESA AIM spacecraft. The instrument capabilities were investigated during the AGEX study, and the measurement principle was demonstrated in the laboratory.

The average gravitational force expected on Dimorphos's surface is around $5 \times 10^{-5} \text{ m s}^{-2}$ (or 5 mGal). Apart from the self-gravitation of the body, centrifugal forces and the acceleration due to the primary (Didymos) contribute to the surface acceleration. In a binary system, the temporal variation due to gravitational interactions, i.e., tides, provides valuable information on dynamics. Temporal variations of the local gravity vector at the landing site will be used to constrain the geological substructure (mass anomalies, local depth, and

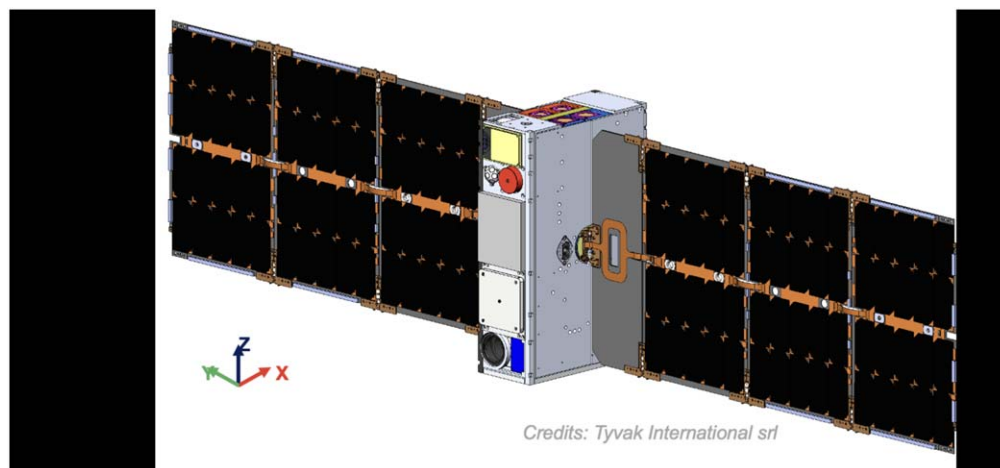


Figure 10. Rendering of the Milani CubeSat.

lateral variations of regolith) and the surface geophysical environment (tides, dynamic slopes, and centrifugal forces).

GRASS has the scientific objectives of determining the local gravity vector with implications on subsurface inhomogeneities and the Dimorphos dynamical state by measuring surface acceleration variations due to rotation kinematics, tides, and orbital dynamics. It will contribute to the global gravity solution, interior structure, and possible surface mass transport.

The gravimeter consists of two axes, each axis with a rotating flat spring, which are accommodated orthogonally in the Juventas CubeSat. This allows the reconstruction of the full three-dimensional local acceleration vector. The gravimeter will be calibrated in situ.

Juventas aims to remain operational on the asteroid surface during at least one orbit of Dimorphos about Didymos, with an extended goal of remaining operational for two full orbits (roughly 24 hr). During this time, GRASS will obtain measurements of the local surface acceleration at the landing site. Multiple measurements (at least 12) will be obtained along each orbit, which enables estimation of the local surface gravity and dynamical state (including libration) of Dimorphos as it orbits the Didymos primary. The gravimeter aims to measure the amplitude of the surface acceleration better than 0.05 mGal with a target accuracy better than 0.002 mGal.

Synergy of data with other instruments on board Juventas and Hera will provide a holistic view of gravity and interior. As the most immediate example, estimates of regolith porosity by JuRa will constrain gravity models for the interior and hence the composition. 3D models of interior structure, if obtained by JuRa, will be overlaid on top of gravity data, giving us crucial information for interior origin and evolution scenarios.

5.7.3. Intersatellite Link for Radio Science

An ISL will be used for Radio Science, allowing the measurement of Didymos's gravity field that cannot be done by Hera alone. The ISL is a crucial add-on to the gravity estimation of low-gravity bodies by exploiting the CubeSat's proximity to the binary, as the range-rate measurements carried out by the intersatellite link contain information on the dynamics of the system, i.e., masses and gravity field of Didymos's primary and secondary. Hera only does not allow the observation of gravity coefficient J_2 of Dimorphos, but with the ISL between HERA and Juventas, it is expected to observe

J_2 with a formal uncertainty of 10%–11%. ISL Ranging and Doppler allows an estimate of higher-degree gravity coefficients of Didymos to degrees 2 and 3. Hera-Juventas ISL is therefore expected to improve the overall accuracy of HERA Radio Science investigation and enables us to estimate the extended gravity field of Didymos and Dimorphos.

5.7.4. GNC Sensor

Juventas is equipped with guidance, navigation, and control (GNC) sensors for autonomous navigation in proximity orbits. These sensors include a visible navigation camera, star trackers (with 15" (1σ) cross-bore-sight and 90" (1σ) around bore-sight accuracy), laser ranger, and sun sensors. Designed for autonomous navigation, these sensors will also be used for context imaging, descent/landing, and attitude determination of Juventas during surface operations over a period of the Dimorphos orbit (11.9 hr) around Didymos that will indicate dynamical variations.

5.7.5. Accelerometers/Gyros

Landing of the Juventas CubeSat will provide a unique opportunity to study surface mechanical properties of an asteroid. The high-frequency data from accelerometers and gyroscopes during the rebounds between the touchdown and final resting position will be analyzed to determine surface strength, in a manner analogous with other small-body landers (e.g., NEAR-Shoemaker, Philae, MASCOT; see O'Rourke et al. 2020, for Philae).

5.8. Milani

Milani is a 6U-sized (six units) CubeSat (Figure 10). It will be deployed after Hera arrival at Didymos to perform independent detailed characterization of Didymos and Dimorphos at distances of 5–10 km, supporting Hera observations and enhancing the overall mission science return. Milani's objectives are to

1. map the global composition of Didymos and Dimorphos;
2. characterize the surface of Didymos and Dimorphos;
3. evaluate DART impact effects and support gravity field determination;
4. characterize dust clouds around the Didymos system.

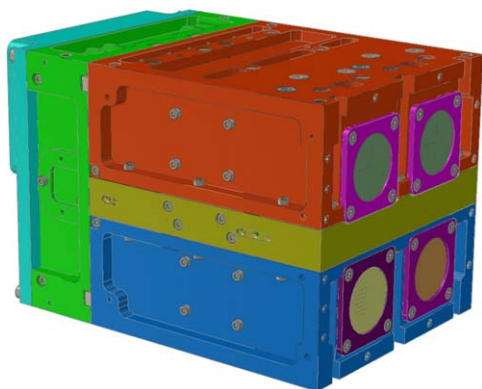


Figure 11. Rendering of the ASPECT hyperspectral imager with its four independent channels and data processing unit (DPU; green).

To achieve these objectives, Milani is carrying two scientific payloads, the ASPECT visual and near-infrared (Vis-NIR) imaging spectrometer and the VISTA thermogravimeter aimed at collecting and characterizing volatiles and dust particles below $10\ \mu\text{m}$. Additionally, navigation payloads include a visible navigation camera and lidar. The Milani consortium is composed of entities and institutions from Italy, the Czech Republic, and Finland. The consortium Prime is Tyvak International, responsible for the whole program management and platform design, development, integration, testing, and final delivery to the customer. Politecnico di Torino is tasked with defining requirements and performing thermal, radiation, and debris analysis. Politecnico di Milano is responsible for mission analysis and GNC. Altec will support the Ground Segment architecture and interface definition. Centro Italiano per la Ricerca Aerospaziale (CIRA) is responsible for the execution of the vehicle environmental campaign. HULD contributes to developing the mission-specific software. VTT is the main payload (ASPECT hyperspectral imager) provider and is supported by the following entities dealing with ASPECT-related development: University of Helsinki (ASPECT calibration); Reaktor Space Lab (ASPECT Data Processing Unit development); Institute of Geology of the Czech Academy of Sciences (ASPECT scientific algorithms requirements and testing); and Brno University of Technology (ASPECT scientific algorithms development). INAF-IAPS is the secondary Payload (VISTA, dust detector) provider.

5.8.1. The ASPECT Hyperspectral Imager

ASPECT is a hyperspectral imaging spectrometer developed by VTT Technical Research Centre of Finland. The ASPECT hyperspectral imager is an evolution of a similar earlier payload on a 3U CubeSat (named identically ASPECT) originally proposed to the AIM mission (Kohout et al. 2018). Its key component is a tunable Fabry–Perot Interferometer (FPI) developed at VTT (Näsilä & Kohout 2020). The FPI consists of two parallel reflective surfaces. The beams of light reflect back and forth between the mirrors, creating constructive interference at certain wavelengths. This allows some wavelengths to be transmitted while others are reflected away. Thus, the interferometer acts as a bandpass filter. By changing the gap between the reflective surfaces, the transmitted wavelength shifts. ASPECT has four measurement channels (Figure 11 and Table 2). VIS and NIR channels have imaging capability, while the SWIR channel is a single-point spectrometer. All channels

Table 2
Key Parameters for ASPECT

Parameter	VIS	NIR1	NIR2	SWRI
FOV	$10^\circ \times 10^\circ$	$6.7^\circ \times 5.4^\circ$	$6.7^\circ \times 5.4^\circ$	5° circular
Spectral range (nm)	500–900	850–1275	1225–1650	1600–2500
Image size (pixels)	1024×1024	640×512	640×512	1 pixel
No. spectral bands	ca. 14	ca. 14	ca. 14	ca. 30
Spectral resolution (nm)	<20	<40	<40	<40

have good overlap, so it is possible to construct the complete spectral slope from 500 up to 2500 nm. Fe^{2+} absorptions, in dry silicates at ~ 1 and $2\ \mu\text{m}$, Fe^{3+} absorptions in hydrated silicates at $\sim 0.7\ \mu\text{m}$, OH^- absorption at $\sim 1.4\ \mu\text{m}$, and H_2O absorption at $\sim 1.9\ \mu\text{m}$ are all found within the ASPECT spectral range.

A dedicated Data Processing Unit (DPU) based on Xiphos Q7S is integrated with ASPECT. The DPU is used to (1) autonomously execute preprogrammed hyperspectral data capture sequences, (2) reconstruct hyperspectral images from the raw data stream and store them in internal memory, (3) run a set of preprogrammed algorithms to autonomously evaluate coverage and sharpness of the hyperspectral data cubes in order to select highest-quality data cubes for download to ground, and (4) compress downloaded data using lossless or near-lossless JPEG2000 compression. These features enable ASPECT imaging strategy based on performing multiple hyperspectral data cube acquisitions of each preselected scene (target asteroid orientation) and downloading the highest-quality data meeting criteria on coverage and sharpness. While we do not intend to update the DPU computer code in flight, the DPU algorithms contain build-in flexible configuration settings to modify or bypass crucial features. The configuration settings can be changed in flight through ground commands enabling optimum algorithm configuration based on actual target appearance (e.g., albedo variations, surface features) and ASPECT imager performance (e.g., noise levels, exposure time).

5.8.2. Volatile In Situ Thermogravimeter Analyser (VISTA)

VISTA is a microthermogravimeter devoted to detection of the presence of dust particles smaller than $5\text{--}10\ \mu\text{m}$, for volatile detection (e.g., water) and light organics characterization (e.g., carboxylic acids with low carbon chain), and to monitoring the molecular outgassing and contamination in support of other instruments. The VISTA instrument is a Piezoelectric Crystal Microbalance (PCM), whose core consists of a couple of piezoelectric quartz crystals (one sensing crystal and the other one for reference), equipped with a built-in metal electrode that acts as a collector of dust and a built-in heater. PCM sensors convert mass changes into fundamental resonance frequency variations according to the Sauerbrey equation (Sauerbrey 1959). VISTA can detect dust particles smaller than a few microns (Palomba et al. 2002) orbiting around the Didymos–Dimorphos system.

VISTA is also equipped with a Thermo-Electric Cooler to decrease the sensor temperature and enhance the contaminant detection. The sensor temperature can be increased in order to

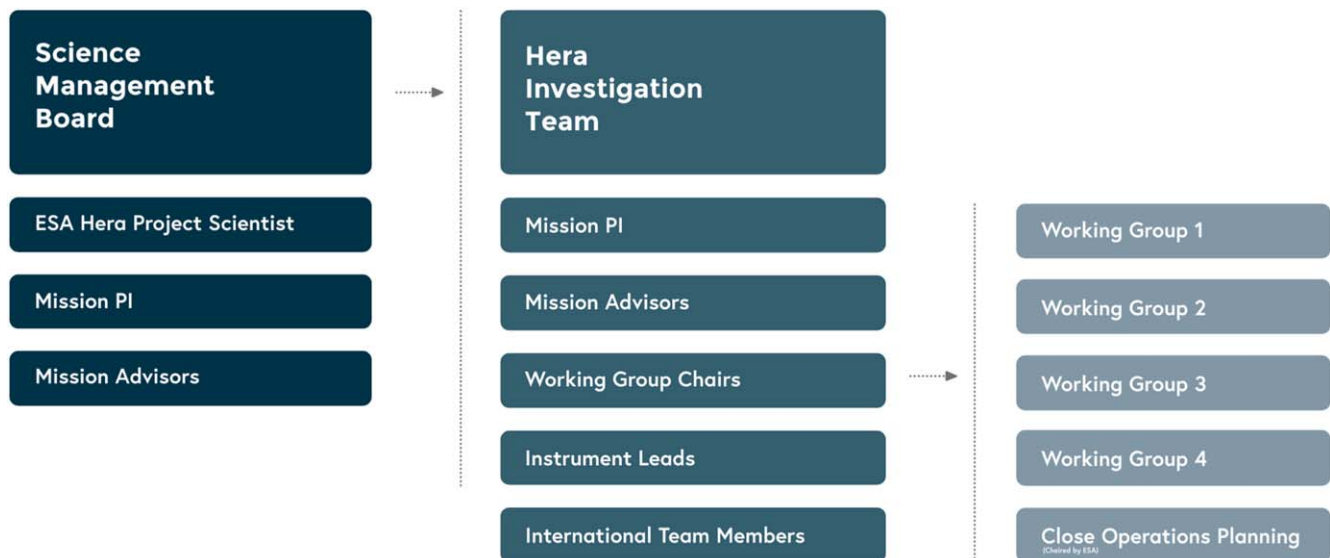


Figure 12. Organization of the Hera Science Team; see also <https://www.heramission.space/team>.

allow the most volatile components of the analyzed sample to desorb. This allows inferring the abundance of the desorbed volatile compound from the mass variation and its composition by measuring its sublimation temperature and its enthalpy of sublimation.

An important challenge of VISTA is the presence of a heater and Resistance Temperature Detector (RTD) integrated onto the crystal. This special design dramatically reduces the instrument mass and the power required to perform thermal cycles to characterize the deposited mass on the sensor head.

6. Mission Organization

The Hera Science Team is structured with a Mission Principal Investigator (PI), a Science Management Board (SMB), and a Hera Investigation Team (HIT), which supervises four Working Groups (WGs). These WGs are defined according to mission topic, which is different from the model adopted for large ESA planetary missions, where the Project Scientist is supported by Science Working Teams consisting mostly of instrument PIs.

The Mission PI is appointed by ESA and is the primary interface to ESA. The Hera SMB consists of the ESA Hera Project Scientist (ESA PS), the Mission PI, and the Hera Advisory Board, consisting of four mission advisors. The Mission PI chairs the HIT and is supported by the Hera Advisory Board.

The tasks of the Hera SMB are

1. advising the Hera mission project team on all aspects related to the Hera mission objectives;
2. ensuring that the WGs' activities cover the needs of the Hera mission;
3. providing recommendations to ESA concerning the membership in the HIT; and
4. implementing the Publication Policy.

The key planetary defense goals of the Hera mission will be achieved through an integrated and coordinated analysis of the payload data retrieved from the Didymos system. To foster this analysis, the remote sensing data analysis will be conducted

under the responsibility of the top-level team of scientists belonging to the HIT.

The HIT consists of

1. the Mission PI;
2. the Hera Advisory Board and WG Chairs;
3. the Hera Instrument Lead; and
4. the Hera International Team Members, who are invited members of the NASA DART, OSIRIS-REx, and/or JAXA Hayabusa2 teams. They support the Hera operations planning and data analysis and interpretation with the experience and tools from previous missions.

Figure 12 shows the organization of the Hera Science Team. The HIT is organized into four WGs as follows:

1. Working Group 1 (WG1): impact modeling.
2. Working Group 2 (WG2): ground-based observations.
3. Working Group 3 (WG3): dynamics and physical properties.
4. Working Group 4 (WG4): data analysis, exploitation, interpretation.

The Hera WG members consist of WG core members and WG extended members. The two types of WG members are distinguished by their involvement in a WG. In addition to these WGs, ESA leads a Close Operations Planning Group.

7. Support from Related European Projects

Since 2012, the European Commission supports projects dedicated to impact hazard and asteroid deflection. Starting in 2012 January, the NEOShield project, which involved 13 international partners, was funded by the FP7 program for 3.5 yr to investigate in detail the three most promising mitigation techniques, the kinetic impactor, blast deflection, and the gravity tractor, and to devise feasible demonstration missions. In addition, the consortium investigated options regarding an international strategy for implementation when an actual impact threat arises. In 2015, building on the foundations of NEOShield, the NEOShield2 project was funded for 2 yr by the Horizon 2020 program to study specific technologies and instruments to conduct close-approach missions to NEOs or to

undertake mitigation demonstration, as well as to acquire in-depth information of physical properties of the population of NEOs between 50 and 300 m, in order to design mitigation missions and assess the consequences of an impact on Earth.

Directly connected to Hera, in 2019, the European Commission funded until the end of 2023 May the NEO-MAPP project (Michel et al. 2021) under the H2020 Research & Innovation Actions call corresponding to “Advanced research in Near Earth Objects (NEOs) and new payload technologies for planetary defense.” NEO-MAPP is an acronym for Near-Earth Object Modeling and Payloads for Protection and is a project that involves 15 partners, including 13 European institutions and 2 European industries (Airbus Defense & Space, GMV) with strong backgrounds in small-body space missions and science. NEO-MAPP is directly relevant to the Hera mission, which has been defined as the reference mission of the project, and most of the European members of the Hera science team (including the PI and the Chairs of WG1, WG3, and WG4) are members of the NEO-MAPP consortium. The project focuses on the following two related topics: (a) maturation or adaptation to specific use cases of existing modeling capabilities regarding the different processes undergone by asteroids (impacts, binary asteroid dynamics, and structural evolution), and (b) development of instruments, technologies, and related data exploitation models to support NEO missions. The project dedicates considerable resources to developing innovative synergies between those two topics.

In line with Hera’s objectives, the main goal of NEO-MAPP is to provide significant advances in our understanding of the response of NEOs to external forces, in particular a kinetic impact like that of DART on Dimorphos, and in associated measurements by a spacecraft, including those necessary for physical characterization. NEO-MAPP activities are thus directly supporting the development of Hera, both in terms of modeling and in terms of hardware development and tools for the analysis of data obtained by the mission. Furthermore, public outreach activities related to Hera, planetary defense, and NEO-MAPP results are an important component of the NEO-MAPP project, given the high public interest for this topic and the need to inspire the younger generation to new challenges and to care about the protection of our planet.

Since the project also includes the development of instruments that are not part of Hera, the NEO-MAPP results and tools will also be of high value for NEO space missions that will follow Hera in the future and for the building of planetary defense road maps.

8. Conclusions and Perspectives

Hera is the European contribution to planetary defense, within a road map that should lead to offering a robust asteroid mitigation plan to future generations. Furthermore, Hera will not only perform the measurements necessary to fully understand the effects of the DART impact on Dimorphos but also provide unique information relevant to many current issues in asteroid science. From small asteroid internal and surface structures, to rubble-pile evolution and impact cratering physics in microgravity, to the long-term effects of space weathering in the inner solar system, to land-form evolution and accretion on small bodies, Hera will have a major impact on many fields of solar system science.

Studies using Hera data will in turn deeply influence our understanding of the asteroid population and, by extension, the population of planetesimals that came together to form the planets, including Earth. The scientific legacy of the Hera mission will extend far beyond the core aims of planetary defense, to help us understand the solar system as a whole.

Hera is the ESA contribution to the AIDA collaboration. Hera, Juventas, Milani, and their instruments are developed under ESA contract supported by national agencies. This project has received funding from the European Union’s Horizon 2020 research and innovation program under grant agreement No. 870377 (project NEO-MAPP), the CNRS through the MITI interdisciplinary programs, ASI, CNES, JAXA, the Academy of Finland project no. 335595, and was conducted with institutional support RVO 67985831 of the Institute of Geology of the Czech Academy of Sciences. M.L., E.P., P.T. and E.D. are grateful to the Italian Space Agency (ASI) for financial support through Agreement No. 2022-8-HH.0 in the context of ESA’s Hera mission. We are grateful to the whole Hera team, including Working Group core members and other contributors for their continuous efforts and support. Their names can be found on the following website: <https://www.heramission.space/team>.

ORCID iDs

Patrick Michel  <https://orcid.org/0000-0002-0884-1993>
 Michael Küppers  <https://orcid.org/0000-0002-5666-8582>
 Benoit Carry  <https://orcid.org/0000-0001-5242-3089>
 Sébastien Charnoz  <https://orcid.org/0000-0002-7442-491X>
 Alan Fitzsimmons  <https://orcid.org/0000-0003-0250-9911>
 Alain Hérique  <https://orcid.org/0000-0003-3699-883X>
 Tomas Kohout  <https://orcid.org/0000-0003-4458-3650>
 Ernesto Palomba  <https://orcid.org/0000-0002-9101-6774>
 Petr Pravec  <https://orcid.org/0000-0001-8434-9776>
 Colin Snodgrass  <https://orcid.org/0000-0001-9328-2905>
 Kleomenis Tsiganis  <https://orcid.org/0000-0003-3334-6190>
 Yun Zhang  <https://orcid.org/0000-0003-4045-9046>
 Sabina D. Raducan  <https://orcid.org/0000-0002-7478-0148>
 Andy F. Cheng  <https://orcid.org/0000-0001-5375-4250>
 Andy Rivkin  <https://orcid.org/0000-0002-9939-9976>
 Olivier Barnouin  <https://orcid.org/0000-0002-3578-7750>
 Carolyn Ernst  <https://orcid.org/0000-0002-9434-7886>
 Angela Stickle  <https://orcid.org/0000-0002-7602-9120>
 Derek C. Richardson  <https://orcid.org/0000-0002-0054-6850>
 Cristina Thomas  <https://orcid.org/0000-0003-3091-5757>
 Akiko Nakamura  <https://orcid.org/0000-0001-6990-8496>
 Makoto Yoshikawa  <https://orcid.org/0000-0002-3118-7475>
 Erik Asphaug  <https://orcid.org/0000-0003-1002-2038>
 Dante S. Lauretta  <https://orcid.org/0000-0002-2597-5950>
 Kevin J. Walsh  <https://orcid.org/0000-0002-0906-1761>

References

- Arakawa, M., Saiki, T., Wada, K., et al. 2020, *Sci*, 368, 67
 Asphaug, E. 2008, *M&PS*, 43, 1075
 Asphaug, E., & Benz, W. 1996, *Icar*, 121, 225
 Asphaug, E., Ryan, E. V., & Zuber, M. T. 2002, in *Asteroids III*, ed. W. F. Bottke et al. (Tucson, AZ: Univ. Arizona Press), 463
 Ballouz, R. L., Walsh, K. J., Barnouin, O. S., et al. 2020, *Natur*, 587, 205
 Barnouin, O. S., Daly, M. G., Palmer, E. E., et al. 2019, *NatGe*, 12, 247
 Belton, M. J. S., Mueller, B. E. A., D’Amario, L. A., et al. 1996, *Icar*, 120, 185
 Benz, W., & Asphaug, E. 1999, *Icar*, 142, 5

- Bierhaus, E. B., Trang, D., & Daly, R. T. 2022, *NatGe*, doi:10.1038/s41561-022-00914-5
- Bottke, W. F., Brož, M., O'Brien, D. P., et al. 2015, in *Asteroids IV*, ed. P. Michel, F. E. DeMeo, & W. F. Bottke (Tucson, AZ: Univ. Arizona Press), 701
- Bottke, W. F., Morbidelli, A., Jedicke, R., et al. 2002, *Icar*, 156, 399
- Bottke, W. F., Nolan, M. C., Greenberg, R., & Kolvoord, R. A. 1994, *Icar*, 107, 255
- Brunetto, R., Loeffler, M. J., Nesvorný, D., Sasaki, S., & Strazzulla, G. 2015, in *Asteroids IV*, ed. P. Michel, F. E. DeMeo, & W. F. Bottke (Tucson, AZ: Univ. Arizona Press), 597
- Buratti, B. J., Britt, D. T., Soderblom, L. A., et al. 2004, *Icar*, 167, 129
- Campo Bagatin, A., Alemañ, R. A., Benavidez, P. G., Pérez-Molina, M., & Richardson, D. C. 2020, *Icar*, 339, 113603
- Campo Bagatin, A., Petit, J. M., & Farinella, P. 2001, *Icar*, 149, 198
- Cardarilli, G. C., Di Nunzio, L., Fazzolari, R., et al. 2019, *Appl. Sci.*, 9, 2909
- Cheng, A. F., Reed, C., Carnelli, I., Michel, P., & Ulamec, S. 2015, *LPSC*, 46, 1386
- Cheng, A. F., Rivkin, A. S., Michel, P., et al. 2018, *P&SS*, 157, 104
- Cho, Y., Morota, T., Kanamaru, M., et al. 2021, *JGRE*, 126, e06572
- Cook, C. M., Melosh, H. J., & Bottke, W. F. 2003, *Icar*, 165, 90
- Daly, R. T., Bierhaus, E. B., Barnouin, O. S., et al. 2020, *GeoRL*, 47, e89672
- Delbo, M., Libourel, G., Wilkerson, J., et al. 2014, *Natur*, 508, 233
- DellaGiustina, D. N., Burke, K. N., Walsh, K. J., et al. 2020, *Sci*, 370, eabc3660
- Dotto, E., Della Corte, V., Amoroso, M., et al. 2021, *P&SS*, 199, 105185
- Farinella, P., Paolicchi, P., & Zappala, V. 1982, *Icar*, 52, 409
- Gassot, O., Herique, A., Fa, W., Du, J., & Kofman, W. 2021, *RaSc*, 56, e07186
- Gladman, B., Michel, P., & Froeschlé, C. 2000, *Icar*, 146, 176
- Gladman, B. J., Migliorini, F., Morbidelli, A., et al. 1997, *Sci*, 277, 197
- Granvik, M., Morbidelli, A., Jedicke, R., et al. 2018, *Icar*, 312, 181
- Grott, M., Knollenberg, J., Hamm, M., et al. 2019, *NatAs*, 3, 971
- Harris, A. W., Galvez, A., Benz, W., et al. 2006, 36th COSPAR Scientific Assembly 36, 2002
- Hergenrother, C. W., Maleszewski, C. K., Nolan, M. C., et al. 2019, *NatCo*, 10, 1291
- Herique, A., Agnus, B., Asphaug, E., et al. 2018, *AdSpR*, 62, 2141
- Herique, A., Kofman, W., Beck, P., et al. 2016, *MNRAS*, 462, S516
- Herique, A., Plettemeier, D., Lange, C., et al. 2019, *AcAau*, 156, 317
- Hirata, N., Barnouin-Jha, O. S., Honda, C., et al. 2009, *Icar*, 200, 486
- Ho, T.-M., Jaumann, R., Bibring, J.-P., et al. 2021, *P&SS*, 200, 105200
- Holsapple, K. A. 1993, *AREPS*, 21, 333
- Holsapple, K. A. 2022, *P&SS*, 219, 105529
- Honda, R., Arakawa, M., Shimaki, Y., et al. 2021, *Icar*, 366, 114530
- Housen, K. R., & Holsapple, K. A. 2003, *Icar*, 163, 102
- Jacobson, S. A., & Scheeres, D. J. 2011, *Icar*, 214, 161
- Jaumann, R., Schmitz, N., Ho, T. M., et al. 2019, *Sci*, 365, 817
- Jawin, E. R., Walsh, K. J., Barnouin, O. S., et al. 2020, *JGRE*, 125, e06475
- Jutzi, M. 2015, *P&SS*, 107, 3
- Kofman, W., Zine, S., Herique, A., et al. 2020, *MNRAS*, 497, 2616
- Kohout, T., Näsiliä, A., Tikka, T., et al. 2018, *AdSpR*, 62, 2239
- La Spina, A., Paolicchi, P., Kryszczyńska, A., & Pravec, P. 2004, *Natur*, 428, 400
- Lagain, A., Bouley, S., Baratoux, D., Costard, F., & Wiczorek, M. 2020, *P&SS*, 180, 104755
- Lauretta, D. S., Adam, C. D., Allen, A. J., et al. 2022, *Sci*, eabm1018
- Lauretta, D. S., DellaGiustina, D. N., Bennett, C. A., et al. 2019, *Natur*, 568, 55
- Lowry, S. C., Fitzsimmons, A., Pravec, P., et al. 2007, *Sci*, 316, 272
- Marchi, S., Chapman, C. R., Barnouin, O. S., Richardson, J. E., & Vincent, J. B. 2015, in *Asteroids IV*, ed. P. Michel, F. E. DeMeo, & W. F. Bottke (Tucson, AZ: Univ. Arizona Press), 725
- Margot, J. L., Nolan, M. C., Benner, L. A. M., et al. 2002, *Sci*, 296, 1445
- Margot, J. L., Pravec, P., Taylor, P., Carry, B., & Jacobson, S. 2015, in *Asteroids IV*, ed. P. Michel, F. E. DeMeo, & W. F. Bottke (Tucson, AZ: Univ. Arizona Press), 355
- Melosh, H. J., Ingram, J., & Bottke, W. F. 1996, *LPSC*, 27, 863
- Melosh, H. J., & Ryan, E. V. 1997, *Icar*, 129, 562
- Michel, P., Ballouz, R. L., Barnouin, O. S., et al. 2020, *NatCo*, 11, 2655
- Michel, P., Benz, W., Tanga, P., & Richardson, D. C. 2001, *Sci*, 294, 1696
- Michel, P., Cheng, A., Küppers, M., et al. 2016, *AdSpR*, 57, 2529
- Michel, P., Kueppers, M., Sierks, H., et al. 2018, *AdSpR*, 62, 2261
- Michel, P., Ulamec, S., & Falke, A. 2021, 43rd COSPAR Scientific Assembly, 312
- Miljković, K., Collins, G. S., Mannick, S., & Bland, P. A. 2013, *E&PSL*, 363, 121
- Murdoch, N., Sánchez, P., Schwartz, S. R., & Miyamoto, H. 2015, in *Asteroids IV*, ed. P. Michel, F. E. DeMeo, & W. F. Bottke (Tucson, AZ: Univ. Arizona Press), 767
- Naidu, S. P., Benner, L. A. M., Brozovic, M., et al. 2020, *Icar*, 348, 113777
- Nakamura, T., Noguchi, T., Tanaka, M., et al. 2011, *Sci*, 333, 1113
- Näsiliä, A., & Kohout, T. 2020, in 2020 IEEE Aerospace Conf. (Piscataway, NJ: IEEE), 1
- Oberbeck, V. R. 1973, *Moon*, 6, 83
- Okada, T. 2020, *Appl. Sci.*, 10, 2158
- Okada, T., Fukuhara, T., Tanaka, S., et al. 2017, *SSRv*, 208, 255
- Okada, T., Fukuhara, T., Tanaka, S., et al. 2020, *Natur*, 579, 518
- O'Rourke, L., Heinisch, P., Blum, J., et al. 2020, *Natur*, 586, 697
- Palomba, E., Colangeli, E. L., Palumbo, P., et al. 2002, *AdSpR*, 29, 1155
- Pravec, P., & Harris, A. W. 2000, *Icar*, 148, 12
- Pravec, P., Vokrouhlický, D., Polishook, D., et al. 2010, *Natur*, 466, 1085
- Raducan, S. D., Davison, T. M., Luther, R., & Collins, G. S. 2019, *Icar*, 329, 282
- Raducan, S. D., & Jutzi, M. 2022, *PSJ*, 3, 128
- Richardson, J. E., Melosh, H. J., Greenberg, R. J., & O'Brien, D. P. 2005, *Icar*, 179, 325
- Rozitis, B., MacLennan, E., & Emery, J. P. 2014, *Natur*, 512, 174
- Rubincam, D. P. 2000, *Icar*, 148, 2
- Sakatani, N., Tanaka, S., Okada, T., et al. 2021, *NatAs*, 5, 766
- Salisbury, J. W., D'Aria, D. M., & Jarosewich, E. 1991, *Icar*, 92, 280
- Sánchez, P., & Scheeres, D. J. 2014, *M&PS*, 49, 788
- Sauerbrey, G. 1959, *ZPhy*, 155, 206
- Sava, P., & Asphaug, E. 2018, *AdSpR*, 61, 2198
- Scheeres, D. 2007, *Icar*, 189, 370
- Scheeres, D. J., Hartzell, C., Sánchez, P., & Swift, M. 2010, *Icar*, 210, 968
- Scheeres, D. J., McMahon, J. W., Bierhaus, E. B., et al. 2021, *LPSC*, 52, 1706
- Scheirich, P., & Pravec, P. 2022, *PSJ*, in press
- Schultz, P. H., Hermalyn, B., & Veverka, J. 2013, *Icar*, 222, 502
- Schwartz, S. R., Richardson, D. C., & Michel, P. 2012, *Granular Matter*, 14, 363
- Shimaki, Y., Senshu, H., Sakatani, N., et al. 2020, *Icar*, 348, 113835
- Statler, T. S. 2009, *Icar*, 202, 502
- Sugita, S., Honda, R., Morota, T., et al. 2019, *Sci*, 364, eaaw0422
- Tatsumi, E., Sugimoto, C., Riu, L., et al. 2021, *NatAs*, 5, 39
- Taylor, M. G. G. T., Altobelli, N., Buratti, B. J., & Choukroun, M. 2017, *RSPTA*, 375, 20160262
- Thomas, P. C., & Robinson, M. S. 2005, *Natur*, 436, 366
- Tortora, P., Gai, I., Lombardo, M., et al. 2020, *EGU General Assembly Conf. Abstracts*, 12800
- Tortora, P., Zannoni, M., Gai, I., et al. 2019, *EPSC*, 13, 1751
- Tortora, P., Zannoni, M., Gramigna, E., et al. 2021, *23rd EGU General Assembly*, EGU21-14898
- Walsh, K. J., Ballouz, R.-L., & Jawin, E. R. 2022, *SciA*, 8, eabm6229
- Walsh, K. J., & Jacobson, S. A. 2015, in *Asteroids IV*, ed. P. Michel, F. E. DeMeo, & W. F. Bottke (Tucson, AZ: Univ. Arizona Press), 375
- Walsh, K. J., Jawin, E. R., Ballouz, R.-L., et al. 2019, *NatGe*, 12, 242
- Walsh, K. J., & Richardson, D. C. 2006, *Icar*, 180, 201
- Walsh, K. J., Richardson, D. C., & Michel, P. 2008, *Natur*, 454, 188
- Watanabe, S., Hirabayashi, M., Hirata, N., et al. 2019, *Sci*, 364, 268
- Wren, P. F., & Fevig, R. A. 2020, in 11th Planetary Crater Consortium, 2251, 2061
- Zannoni, M., Gai, I., Lombardo, M., et al. 2020, *EPSC*, 14, 691
- Zannoni, M., Tommei, G., Modenini, D., et al. 2018, *AdSpR*, 62, 2273
- Zhang, Y., & Michel, P. 2020, *A&A*, 640, A102
- Zhang, Y., Michel, P., Richardson, D. C., et al. 2021, *Icar*, 362, 114433
- Zhang, Y., Richardson, D. C., Barnouin, O. S., et al. 2017, *Icar*, 294, 98